Bioorthogonal Activation of Photosensitizer with Extrinsic Enzyme for Precisive Photodynamic Therapy

Junlong Xiong,[†,#] Jacky C. H. Chu,[†,#] Wing-Ping Fong,[‡] Clarence T. T. Wong,*[§] and Dennis K. P. Ng*[†]

[†] *Department of Chemistry, The Chinese University of Hong Kong, Shatin, N.T., Hong Kong, China*

[‡] *School of Life Sciences, The Chinese University of Hong Kong, Shatin, N.T., Hong Kong, China*

[§] *Department of Applied Biology and Chemical Technology and State Key Laboratory of Chemical Biology and Drug Discovery, The Hong Kong Polytechnic University, Hung Hom, Kowloon, Hong Kong, China*

[#] *These authors contributed equally to this work*

ABSTRACT: Delivery of functional proteins into the intracellular space has been a challenging task that could lead to a myriad of therapeutic applications. We report herein a novel bioconjugation strategy for enzyme modification and selective delivery into cancer cells for bioorthogonal activation of photosensitizers. By using a bifunctional linker containing a bis(bromomethyl)phenyl group and an *o*-phthalaldehyde moiety, it could induce cyclization of the peptide sequence Ac-NH-CRGDfC-$CONH_2$ through site-specific dibenzylation with the two cysteine residues and further coupling with β-galactosidase via the phthalaldehyde-amine capture reaction. This facile two-step one-pot procedure enabled the preparation of cyclic RGD-modified β-galactosidase readily, which could be internalized selectively into $\alpha_v\beta_3$ integrin-overexpressed cancer cells. Upon encountering an intrinsically quenched distyryl boron dipyrromethene-based photosensitizer conjugated with a galactose moiety through a self-immolative linker inside the cells, the extrinsic enzyme induced specific cleavage of the β-galactosidic bond followed by self-immolation to release an activated derivative, thereby restoring the photodynamic activities and causing cell death effectively. The high specificity of this extrinsic enzyme-activated photosensitizing system was also demonstrated in vivo using nude mice bearing an $\alpha_v\beta_3$ integrin-positive U87-MG tumor. The bioorthogonal activation at the tumor site resulted in lighting up and complete eradication of the tumor upon laser irradiation, while by using the native β-galactosidase the effects were largely reduced. In contrast to the conventional activation using intrinsic enzymes, this extrinsic enzyme activatable approach can further minimize the nonspecific activation toward precisive photodynamic therapy.

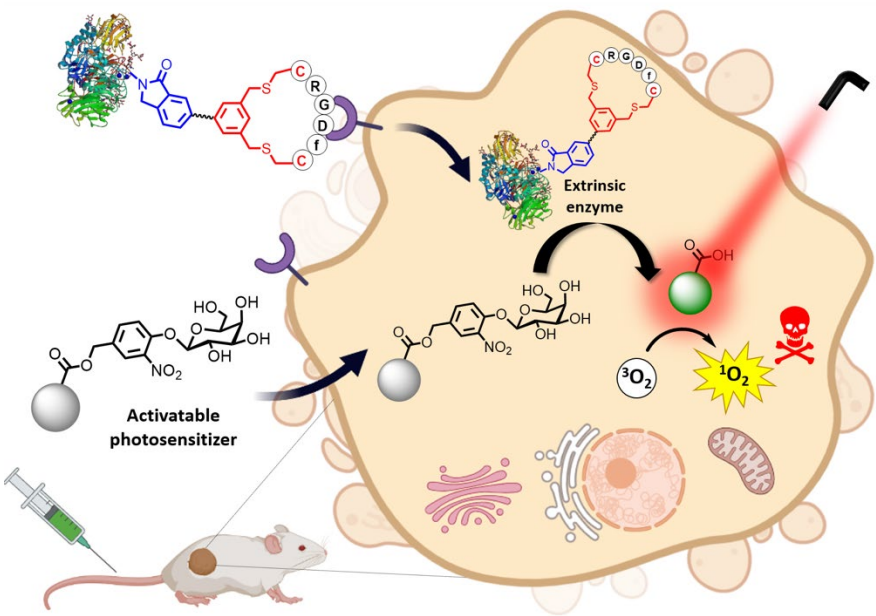
Extrinsic enzyme
Activatable photosensitizer
$^3O_2$
$^1O_2$

INTRODUCTION

Photodynamic therapy (PDT) is a clinically approved treatment modality for a range of cancers and certain noncancerous conditions.[1-3] It involves the photochemical reaction of a photosensitizer and endogenous oxygen to generate highly cytotoxic reactive oxygen species (ROS) for eradication of the cancer cells and tissues. Compared with the conventional anticancer modalities, PDT is less invasive and induces fewer side effects. It also exhibits spatiotemporal selectivity and negligible drug resistance. These advantages render this treatment procedure a promising approach for combating various malignancies. However, the specificity of the photodynamic action remains as an issue that greatly determines the treatment outcome. As a result, there has been considerable interest in the development of advanced photosensitizing systems that can achieve targeted delivery to and controlled ROS generation at the tumor site.[4-6]

To enhance the localization in tumor, a wide range of tumor-targeting ligands, such as biotin, folate, aptamers, peptides, and antibodies have been conjugated to the photosensitizers.[7,8] Although this approach can generally promote the uptake by cancer cells, the "always-on" nature of these photosensitizers may cause phototoxicity at the nontarget sites due to the nonspecific uptake. In attempts to circumventing this problem, stimuli-responsive photosensitizers have been developed.[9-11] These smart therapeutic agents are generally deactivated in their native form by various quenching mechanisms, but upon interactions with stimuli in the tumor microenvironment, such as the slightly acidic and thiol-enriched conditions and the proteases overexpressed in cancer cells, their photodynamic activities can be restored. This approach can potentially minimize the photodamage to normal cells and tissues.

Various intracellular proteases have been utilized as stimuli to activate the photodynamic action of photosensitizers.[9] NAD(P)H:quinone oxidoreductase isozyme 1, for example, has been used to trigger the release of photosensitizers in polymeric nanovesicles inside the cancer

cells, leading to restoration of their photoactivities.[12] However, although this enzyme is overexpressed in many types of tumors, it is also highly expressed in the liver and adipocytes.[13] Similarly, a series of matrix metalloproteinase-activated photosensitizers have been reported which show preferential activation in tumors.[14,15] Although these enzymes are overexpressed in pancreatic, colon, breast, and non-small-cell lung cancers, they are also present in most epithelial cells.[16] In addition, while cathepsin B has also been used to activate various prodrugs, fluorescent probes, and photosensitizers,[17,18] it is also overproduced in the lysosomes of many types of cells.[19] To the best of our knowledge, all the enzyme-activated photosensitizers reported so far require the intrinsic enzymes for activation. As a result of the relatively small difference in the expression levels between the cancer cells and the normal cells, it is inevitable to result in off-target activation of the phototoxicity, leading to undesired side effects (Figure 1a).

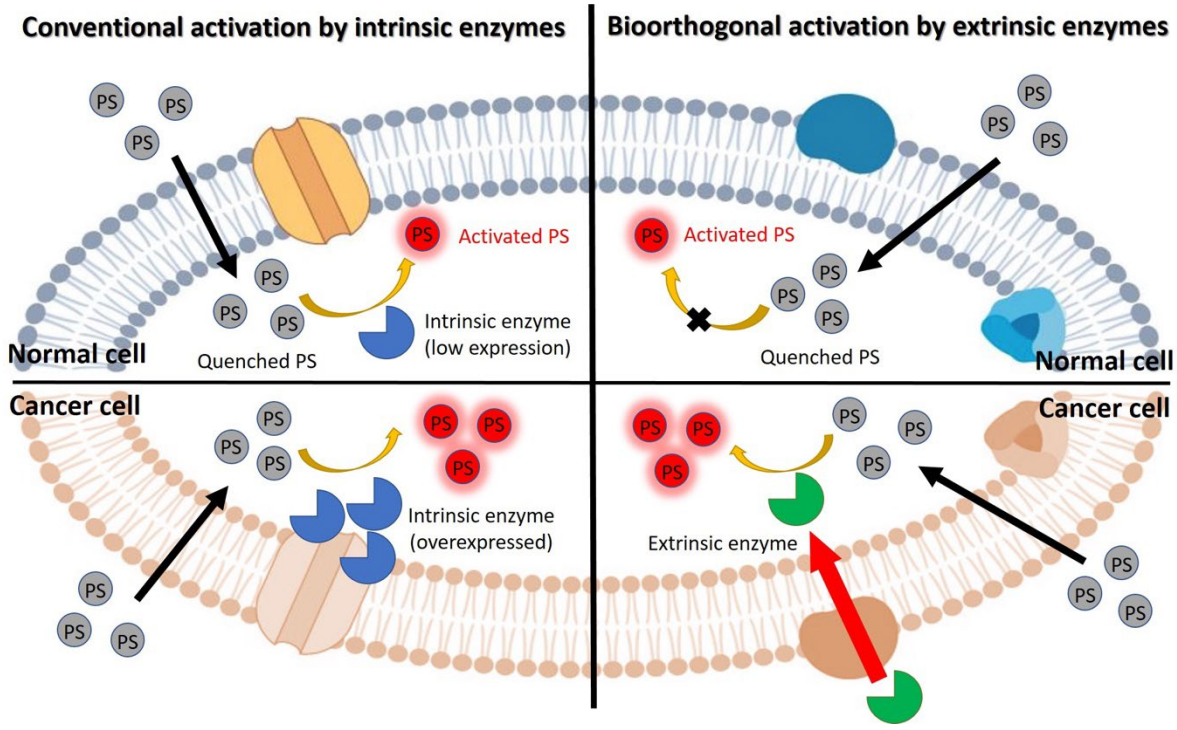

Figure 1. Schematic diagram illustrating the difference in the activation mechanism between the conventional intrinsic enzyme-activated and the bioorthogonal extrinsic enzyme-activated systems.

To overcome the drawback of intrinsic enzyme-activated photosensitizers, we report herein a novel bioorthogonal approach using an extrinsic enzyme for activation. This extrinsic enzyme-activated photosensitizing system involves two bioorthogonal components, namely an extrinsic enzyme modified with tumor-targeting moieties and the corresponding substrate conjugated with a photosensitizer that can be activated upon the enzymatic cleavage. As the normal cells would not have this extrinsic enzyme, the unwanted activation in these cells is negligible, which can minimize the background fluorescence signal and the photocytotoxicity against these cells. In contrast, as the extrinsic enzyme is selectively delivered into the cancer cells through the directing effect of the tumor-targeting moieties, the activation in these cells is remarkable (Figure 1b). Hence, this bioorthogonal activation strategy using extrinsic enzymes as stimuli is more tumor-specific than the conventional activation by intrinsic enzymes.

Figure 2 illustrates the mechanistic action of this extrinsic enzyme-activated photosensitizing system. β-Galactosidase (β-Gal), which is a common biomarker of cell senescence,[20] was chosen as the stimulus. While this lysosomal glycoside hydrolase enzyme is closely associated with the primary ovarian cancer,[21,22] it is not a biomarker of other cancers and hence serves as a suitable candidate of extrinsic enzymes. To selectively deliver this enzyme into the cancer cells, it was modified with cyclic RGD peptide moieties that can target the $\alpha_v\beta_3$ integrin upregulated on most cancer cells,[23] using our previously reported peptide cyclization strategy[24-26] and phthalaldehyde-amine capture (PAC) reaction.[27,28] It is worth mentioning that proteins are generally impermeable to the cells due to their high molecular weight. Various carriers, such as nanoparticles, polymers, and liposomes have been utilized to assist the trafficking across the plasma membrane.[29-31] Cell-penetrating peptides have also been introduced for this purpose through protein expression,[29,32] covalent conjugation,[33] or host-guest interactions.[34] However, to the best of our knowledge, protein delivery into target cells

mediated by direct conjugation with tumor-targeting ligands has not been reported so far. For the activatable photosensitizing component, a distyryl boron dipyrromethene (DSBDP) was conjugated with a galactose moiety through a self-immolative linker. Upon internalization, this deactivated photosensitizer would undergo enzymatic cleavage by the extrinsic enzyme followed by self-immolation to release an activated form of DSBDP, leading to restoration of the fluorescence emission and ROS generation. Photodynamic eradication of cancer cells can therefore be achieved in a precisive manner. It is noteworthy that although there are many examples of β-Gal-responsive fluorescent probes,[21,22] β-Gal-activated photosensitizers have rarely been reported.[35] In addition, activation of photosensitizers inside the cancer cells in a bioorthogonal fashion is also little studied.[36,37]

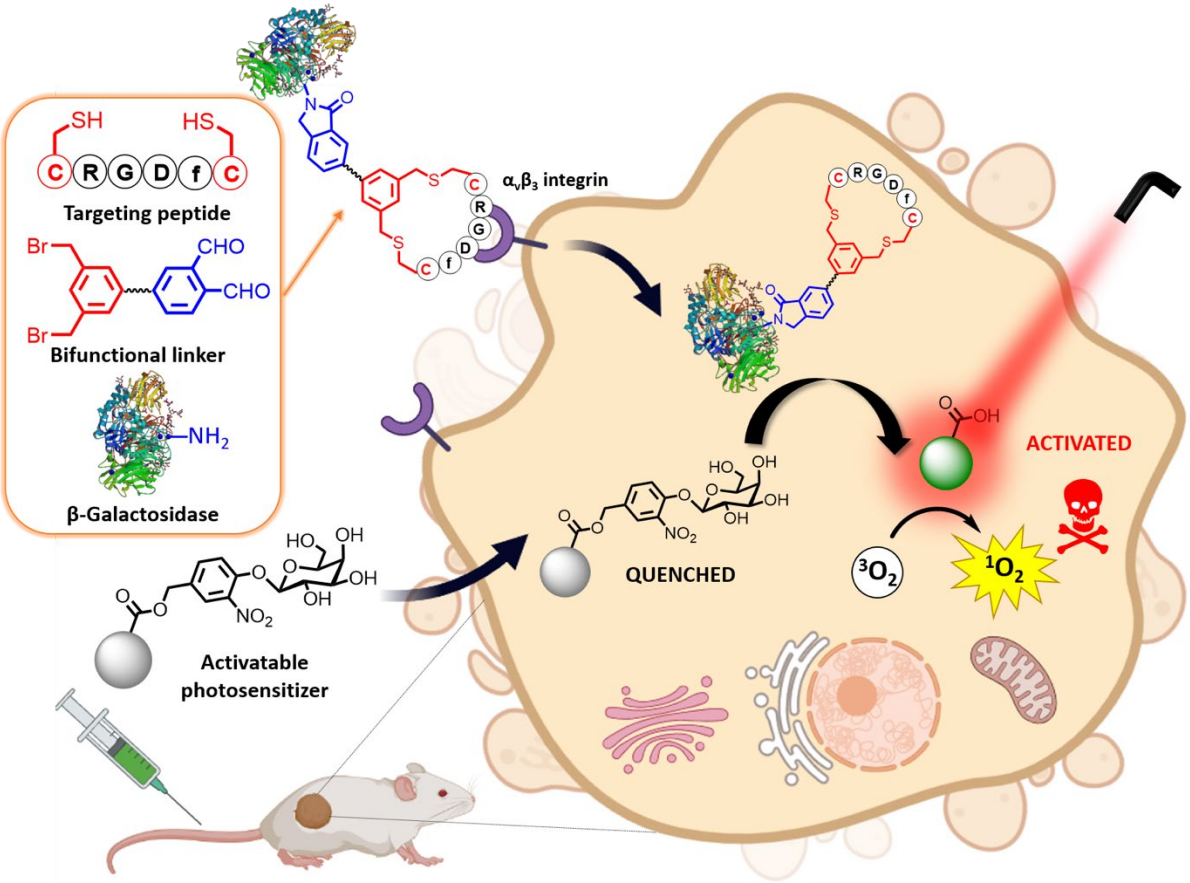

Figure 2. Schematic diagram illustrating the working principle of the bioorthogonally extrinsic enzyme-activated photosensitizing system.

RESULTS AND DISCUSSION

Cyclic Peptide Conjugation and Targeted Delivery of Green Fluorescent Protein. To demonstrate that the bioligation method can be used to prepare functional proteins that can be delivered selectively into cancer cells, green fluorescent protein (GFP) was first chosen as a model substrate because of its impermeability through the cell membrane and strong fluorescence that can facilitate the visualization using confocal fluorescence microscopy. As shown in Figure 3a, the bifunctional linker **1**, which was prepared according to our previously described procedure,[28] was treated with a mixture of trifluoroacetic acid (TFA) and water (1:1 v/v) to remove the acetal protecting group, followed by coupling with the linear peptide AcNH-CMYIEALDRYAC-$COHN_2$ (labeled as **EBP**) via site-specific dibenzylation with the two cysteine residues in borate buffer (pH 8.5, 1 mM). The resulting cyclic **EBP**-conjugated *o*-phthalaldehyde (labeled as **cEBP-OPA**) could be purified readily by high-performance liquid chromatography (HPLC) and characterized by matrix-assisted laser desorption/ionization time-of-flight (MALDI-TOF) mass spectrometry (Figure S1 in the Supporting Information). The cyclic EBP peptide was selected because of its high and selective affinity toward the epidermal growth factor receptor (EGFR), which is overexpressed in a wide range of cancer cells.[25] Without prior purification, this compound was conjugated with GFP (5 μM) in phosphate-buffered saline (PBS) (pH 7.4) in a 20:1 mole ratio via the PAC reaction.[27] After stirring for 30 min at room temperature, the mixture was filtered using a 3 kDa cut-off membrane filter to give the cyclic peptide-conjugated protein **cEBP-GFP**, which was characterized using sodium dodecyl sulfate-polyacrylamide gel electrophoresis (SDS-PAGE) (Figure S2 in the Supporting Information). This one-pot bioligation methodology has previously been used by us to prepare cyclic RGD-conjugated red blood cells for targeted delivery of photosensitizers.[28] We now extend it to synthesize cyclic peptide-conjugated proteins.

The selective uptake of **cEBP-GFP** by EGFR-overexpressed cancer cells was then examined using confocal microscopy. Three cell lines, including the EGFR-positive A549 human lung carcinoma cells[38] and HT29 human colorectal adenocarcinoma cells,[25] and the EGFR-negative HeLa human cervical carcinoma cells[25] were incubated with **cEBP-GFP** or the native GFP (both at 0.1 mM) used as a negative control for 1 h. The confocal images (Figure 3b) clearly showed that the native GFP was unable to enter into the intracellular space of all the three cell lines. In contrast, **cEBP-GFP** could be selectively internalized into the EGFR-positive A549 and HT29 cells, but not the EGFR-negative HeLa cells, as reflected by the intracellular fluorescence intensity. The results clearly indicated that this protein modification method could be used to deliver proteins into the targeted cells. As GFP can emit fluorescence only when it has a correctly folded protein structure, the strong fluorescence observed inside the EGFR-positive cancer cells suggested that the protein structure of GFP was retained after the modification.

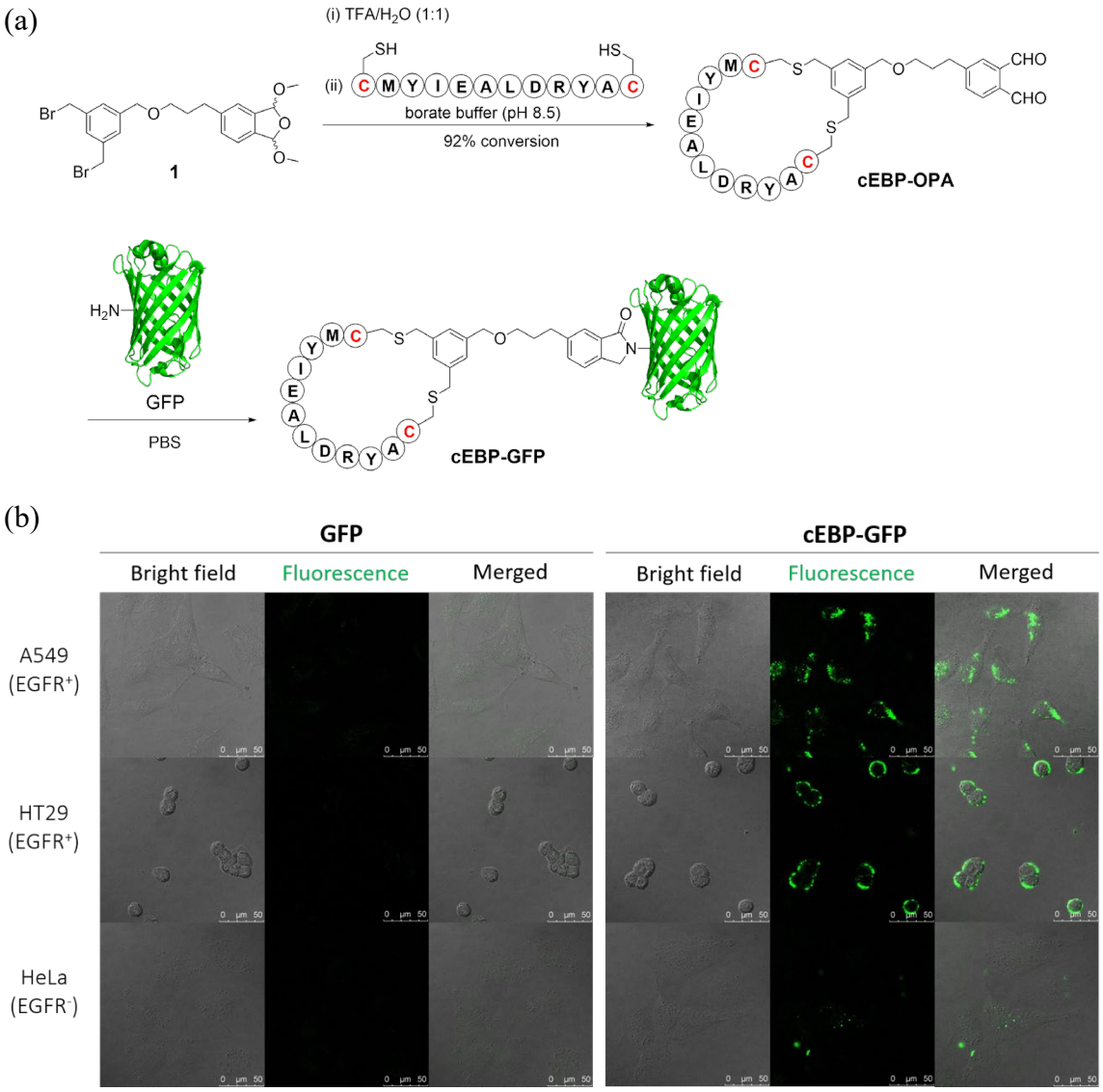

Figure 3. (a) Synthetic scheme of the one-pot peptide cyclization and conjugation with GFP. (b) Bright field, fluorescence, and the merged images of A549, HT29, and HeLa cells after incubation with GFP or **cEBP-GFP** (both at 0.1 mM) for 1 h.

Synthesis and Characterization of cRGD-β-Gal and gal-DSBDP. Based on these encouraging results, we modified β-Gal with another tumor-targeting peptide against the $\alpha_v\beta_3$ integrin. Similarly, treatment of the bifunctional linker **1** with TFA/water (1:1 v/v) followed by coupling with AcNH-CRGDfC-$CONH_2$ gave the cyclic peptide-conjugated *o*-phthalaldehyde **cRGD-OPA**, which was further coupled with β-Gal according to the above procedure to afford

cRGD-β-Gal (Figure 4a). **cRGD-OPA** was purified by HPLC and characterized by MALDI-TOF mass spectrometry, while the successful formation of **cRGD-β-Gal** was confirmed by SDS-PAGE analysis (Figure S3 and S4 in the Supporting Information, respectively).

For the β-Gal-responsive photosensitizing component, a DSBDP-based photosensitizer was used owing to their superior photosensitizing properties.[39] It has been reported that the photophysical properties of these dyes are greatly affected by the meso substituent, and by converting an ester group to a carboxylate moiety at this position, both the fluorescence emission and ROS generation can be greatly enhanced.[40] Based on this "ester-to-carboxylate" effect, we synthesized a DSBDP-based photosensitizer that can be activated by β-Gal. As shown in Figure 4b, reduction of the galactoside-linked benzaldehyde **2**[41] with $NaBH_4$ gave the corresponding benzyl alcohol **3**, which underwent bromination with PBr_3 to afford the galactosylated benzyl bromide **4**. For the DSBDP part, boron dipyrromethene **5**[42] was iodinated with *N*-iodosuccinimide (NIS) to give the diiodo derivative **6**, which then underwent Knoevenagel condensation with excess triethylene glycol monomethyl ether-substituted benzaldehyde **7**[43] to afford DSBDP **8**. The two triethylene glycol chains were introduced to improve the water solubility, biocompatibility, and cellular uptake of the photosensitizer.[44] BODIPY **8** was then hydrolyzed with LiI in ethyl acetate to give the carboxy DSBDP **9**, which was then coupled with the galactosylated benzyl bromide **4** to afford the substituted product **10**. Upon hydrolysis with K_2CO_3 in a mixture of MeOH and $CHCl_3$ (1:10 v/v), the acetyl groups of **10** were removed, giving the target compound **gal-DSBDP**. The characterization data for all the new compounds are given in the Supporting Information.

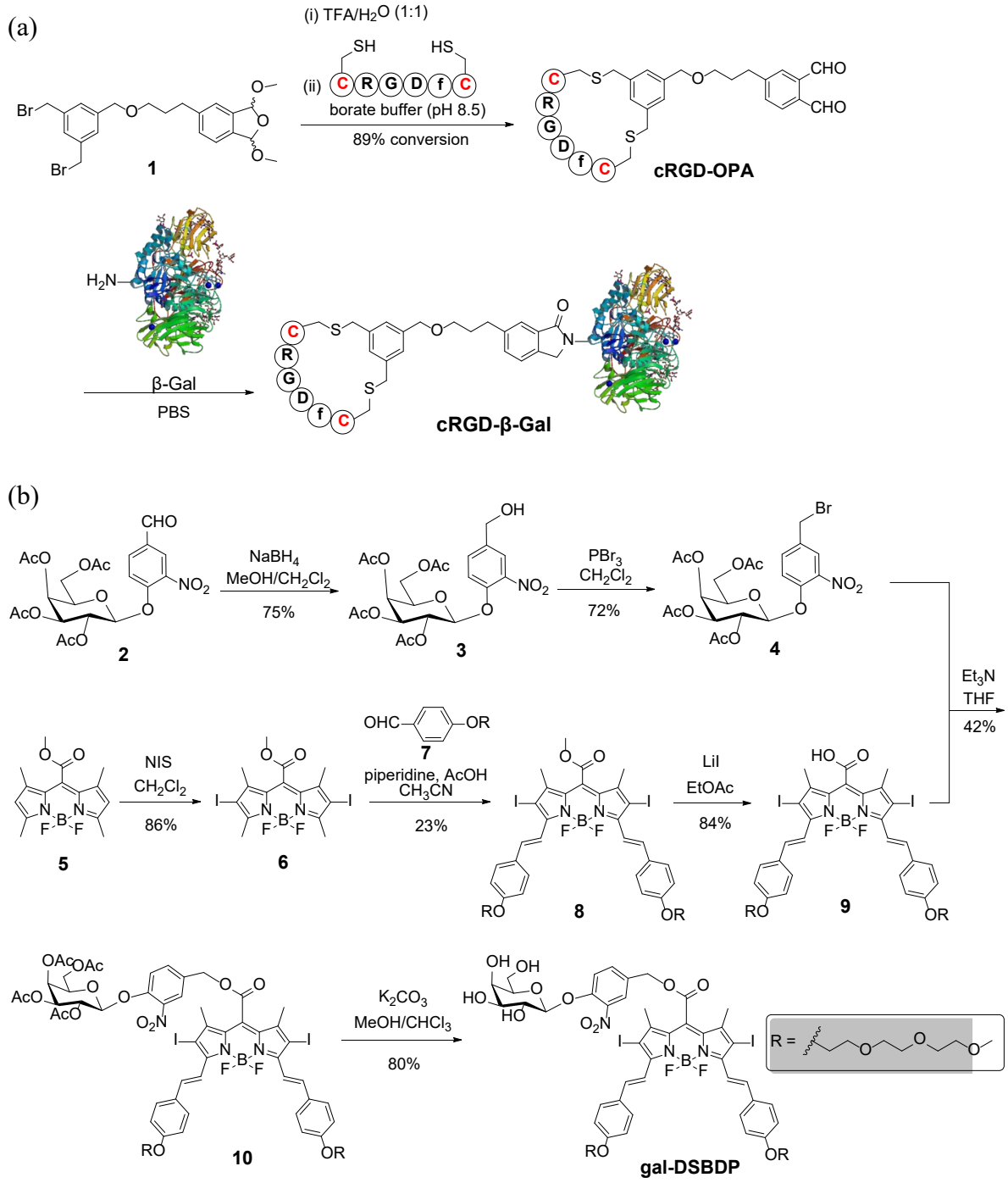

Figure 4. Synthetic schemes of (a) **cRGD-β-Gal** and (b) **gal-DSBDP**.

Photophysical Properties and Enzymatic Activation of gal-DSBDP. The electronic absorption and fluorescence spectra of **gal-DSBDP** were recorded in PBS (pH 7.4) with 10% dimethylsulfoxide (DMSO) (v/v) and compared with those of **9**, which is the expected product after enzymatic activation (Figure S5 in the Supporting Information). While the absorption

spectrum of **9** exhibited an intense absorption at 651 nm, this absorption band was split, broadened, and red-shifted (to 710 nm for the longest-wavelength absorption) for **gal-DSBDP** as observed previously for related DSBDPs.[42] Upon excitation at 610 nm, **9** showed a strong fluorescence band at 685 nm with a fluorescence quantum yield (Φ_f) of 0.14 relative to zinc(II) phthalocyanine [$\Phi_F = 0.28$ in *N*,*N*-dimethylformamide (DMF)].[18] In contrast, **gal-DSBDP** was essentially non-emissive ($\Phi_F = 0.01$), showing that the fluorescence of **gal-DSBDP** was almost completely quenched by caging the meso carboxylate of the DSBDP core. These spectral data are summarized in Table S1 in the Supporting Information.

The activation of **gal-DSBDP** by β-Gal was first studied by monitoring the changes in the electronic absorption and fluorescence spectra of **gal-DSBDP** (2 μM) upon incubation with β-Gal (6 unit mL^{-1}) in PBS (pH 7.4) with 10% DMSO (v/v) at 37 ºC. It was found that the longer-wavelength absorption band at 710 nm diminished and the shorter-wavelength absorption band at ca. 650 nm increased in intensity over a period of 3 h with a clear isosbestic point at ca. 680 nm (Figure 5a), indicating that the enzymatic reaction proceeded efficiently without generating any side products. As expected, the fluorescence intensity increased significantly over this period of time (Figure 5b), and the intensity after the treatment for 3 h was higher when the concentration of β-Gal was increased (from 0 to 6 unit mL^{-1}) (Figure 5c). It is clear that the fluorescence emission of **gal-DSBDP** could be activated by β-Gal. For the cyclic RGD-modified analogue **cRGD-β-Gal**, it could also trigger the fluorescence emission of **gal-DSBDP**. By monitoring the fluorescence intensity at 685 nm at different incubation time, it was found that rate of fluorescence enhancement was comparable for β-Gal and **cRGD-β-Gal** (Figure S6 in the Supporting Information), showing that the enzymatic activity of β-Gal was not reduced after the chemical modification. Moreover, the activation was found to be very selective. As shown in Figure 5d, only upon the treatment with β-Gal, the fluorescence of **gal-DSBDP** could be restored. The presence of other common interfering species, including

$MgCl_2$, $CaCl_2$, homocysteine (Hcy), cysteine (Cys), dithiothreitol (DTT), glutathione (GSH), vitamin C, and H_2O_2 could not induce observable changes.

Apart from fluorescence emission, the singlet oxygen generation of **gal-DSBDP** could also be restored upon treatment with β-Gal. By using 1,3-diphenylisobenzofuran (DPBF) as the singlet oxygen scavenger,[18] the singlet oxygen generation efficiency of **gal-DSBDP** was studied both before and after the treatment with β-Gal. As shown in Figure 5e, the absorbance of the DPBF's absorption at 417 nm was essentially unchanged for **gal-DSBDP** upon irradiation ($\lambda > 610$ nm), showing that the singlet oxygen generation of this dye was largely inhibited. However, after the treatment with β-Gal (6 unit mL^{-1}) in PBS (pH 7.4) with 10% DMSO (v/v) at 37 °C for 3 h, the absorbance decreased rapidly along with the irradiation time, and the rate was very similar to that for the carboxy derivative **9**, indicating the full activation in singlet oxygen generation.

The activation in fluorescence emission and singlet oxygen generation could be attributed to the "ester-to-carboxylate" conversion[42] induced by β-Gal as depicted in Figure 5f. Having an ester substituent at the meso position, **gal-DSBDP** was in a deactivated form. Upon specific enzymatic cleavage of the β-galactosidic bond by β-Gal, a labile intermediate was expected to be formed which underwent self-immolation to give the carboxy derivative **9**, thereby restoring these photoactivities. To confirm the conversion of **gal-DSBDP** to **9** upon the treatment with β-Gal, HPLC analysis was performed for the reaction mixture. After treating **gal-DSBDP** with β-Gal for 1 h, a new peak was observed in the chromatogram, of which the retention time was essentially the same as that for **9**, and the intensity of this peak became higher when the reaction time was prolonged to 3 h (Figure S7a in the Supporting Information). This fraction was collected and analyzed by electrospray ionization (ESI) mass spectrometry. The base peak at *m*/*z* 1067.1448 could be assigned to the $[M+Na]^+$ ions of **9** (Figure S7b in the Supporting Information). These results supported the activation mechanism proposed in Figure 5f.

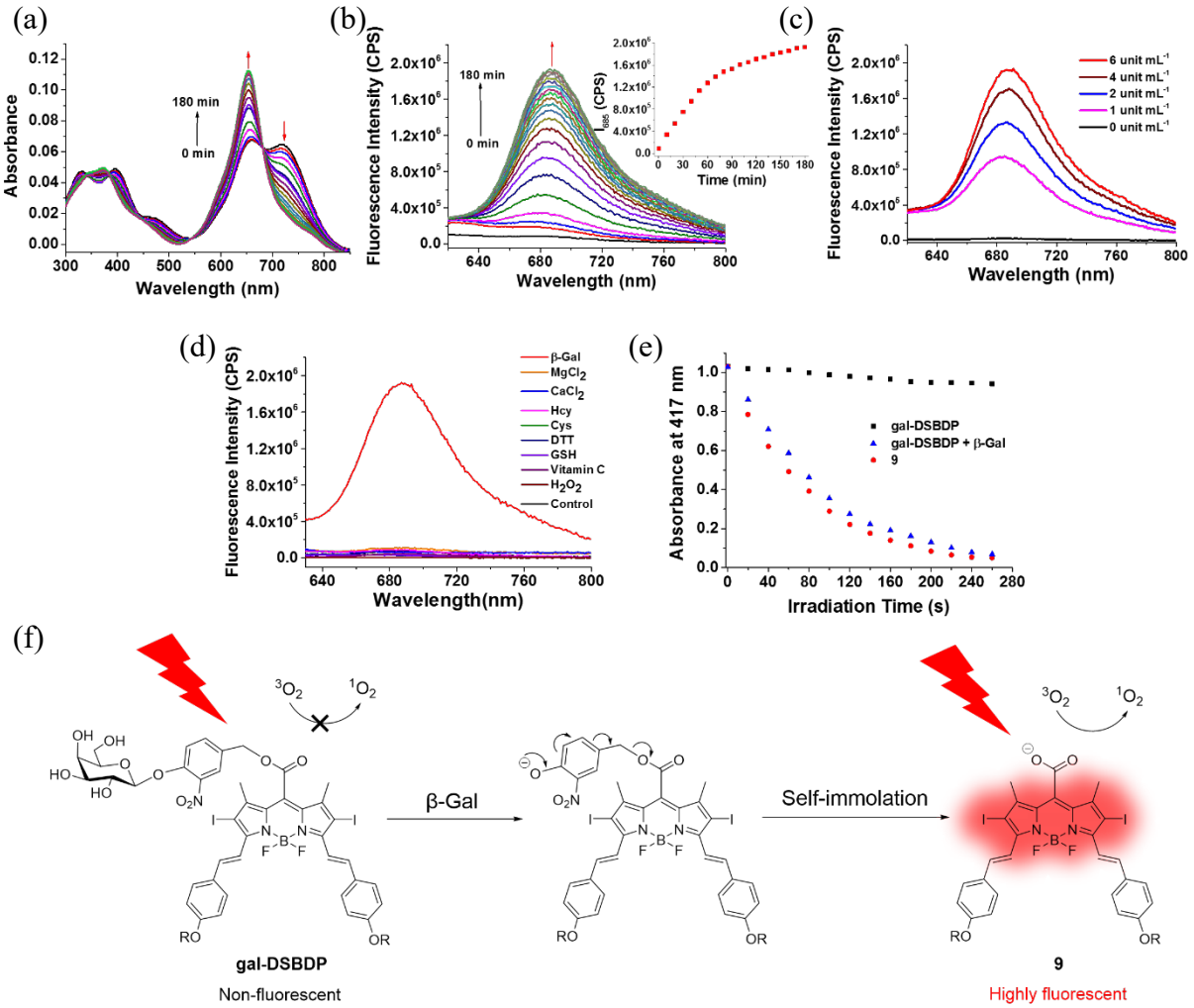

Figure 5. Changes in (a) electronic absorption and (b) fluorescence (λ_{ex} = 610 nm) spectra of **gal-DSBDP** (2 μM) in the presence of β-Gal (6 unit mL^{-1}) in PBS (pH 7.4) with 10% DMSO (v/v) at 37 °C over a period of 3 h. (c) Fluorescence spectra (λ_{ex} = 610 nm) of **gal-DSBDP** (2 μM) after the treatment with various concentrations of β-Gal (0-6 unit mL^{-1}) for 3 h in PBS (pH 7.4) with 10% DMSO (v/v) at 37 °C. (d) Fluorescence spectra (λ_{ex} = 610 nm) of **gal-DSBDP** (2 μM) in the absence or presence of β-Gal (6 unit mL^{-1}) or various interfering species (1 mM) after 3 h in PBS (pH 7.4) with 10% DMSO (v/v) at 37 °C. (e) Comparison of the rates of decay of DPBF sensitized by **9** and **gal-DSBDP** (both at 2 μM) with or without the treatment with β-Gal (6 unit mL^{-1}) in PBS (pH 7.4) with 10% DMSO (v/v) at 37 °C for 3 h upon irradiation (λ > 610 nm). (f) Proposed activation mechanism of **gal-DSBDP** by β-Gal.

In Vitro Studies. The bioorthogonal activation of **gal-DSBDP** by the extrinsic **cRGD-β-Gal** was then studied at the cellular level by confocal microscopy and flow cytometry, using a range of cell lines with different expression levels of $\alpha_v\beta_3$ integrin, including the integrin-positive U87-MG human glioblastoma cells[24,28] and MDA-MB-231 human breast adenocarcinoma cells,[45] as well as the integrin-negative MCF-7 human breast adenocarcinoma cells[24,28,45] and HEK-293 human embryonic kidney normal cells.[28,45] These cells were incubated with **gal-DSBDP** (4 μM) for 30 min with or without pretreatment with **cRGD-β-Gal** or β-Gal (10 unit mL^{-1}) for 1 h, followed by post-incubation in a drug-free medium for further 3 h to provide sufficient time for the intracellular enzymatic reaction. As shown in the confocal images (Figure 6a), noticeable fluorescence could only be observed for the integrin-positive U87-MG and MDA-MB-231 cells being pretreated with **cRGD-β-Gal**. For all the other conditions, the intracellular fluorescence remained very weak. Similar results were obtained by flow cytometry (Figure 6b). The U87-MG cells with pretreatment with **cRGD-β-Gal** (10 unit mL^{-1}) showed the highest intracellular fluorescence intensity, which was ca. 8.5-fold higher than that for HEK-293 cells being treated similarly. The use of a lower concentration of enzyme (2 unit mL^{-1}) could not significantly increase the fluorescence intensity. These results indicated that the cyclic RGD peptide moieties could mediate the internalization of **cRGD-β-Gal**, thereby enabling the activation of **gal-DSBDP** inside the integrin-positive cancer cells. As β-Gal does not exist intrinsically in these cells and the native form of this enzyme cannot be internalized, incubation with this enzyme could not lead to bioorthogonal activation intracellularly.

The in vitro photodynamic activity of this extrinsic enzyme-activated photosensitizing system was also investigated against the integrin-positive U87-MG cells and the integrin-negative MCF-7 cells by the MTT [MTT = 3-(4,5-dimethylthiazol-2-yl)-2,5-diphenyl-tetrazolium bromide] assay. Figure 6c shows the cell viability curves for **gal-DSBDP** against

these two cell lines with pre-incubation with different concentrations of **cRGD-β-Gal**. In the absence of light, the treatment did not cause significant cytotoxicity toward the two cell lines regardless of the enzyme concentration used for the pretreatment. Upon light irradiation ($\lambda >$ 610 nm, 23 mW cm^{-2}, 28 J cm^{-2}), the cell viability was slightly dropped for the MCF-7 cells (to ca. 80% when 20 unit mL^{-1} of **cRGD-β-Gal** was used). In contrast, for the U87-MG cells, the cell viability was decreased significantly, and the extent was increased with the enzyme concentration. The cells were almost completely killed when they were pretreated with 20 unit mL^{-1} of **cRGD-β-Gal**. The remarkable difference in the intracellular fluorescence intensity and the photocytotoxicity between the positive results and the negative controls demonstrated the high specificity of this strategy in bioimaging and PDT.

It is worth mentioning that there are only a few examples of molecular-based bioorthogonally activated photosensitizers that can be excited with light in the near-infrared biological window.[6] Although meso-ester-substituted DSBDP-based photosensitizers have been applied for detection of the endogenous peroxynitrite and hydrogen peroxide in cells,[46,47] the use of extrinsic enzymes that have been delivered into the cells from an external source as stimuli for this class of near-infrared-absorbing activatable photosensitizers has not been reported so far, and this activation strategy should be more specific that the activation by intrinsic stimuli.

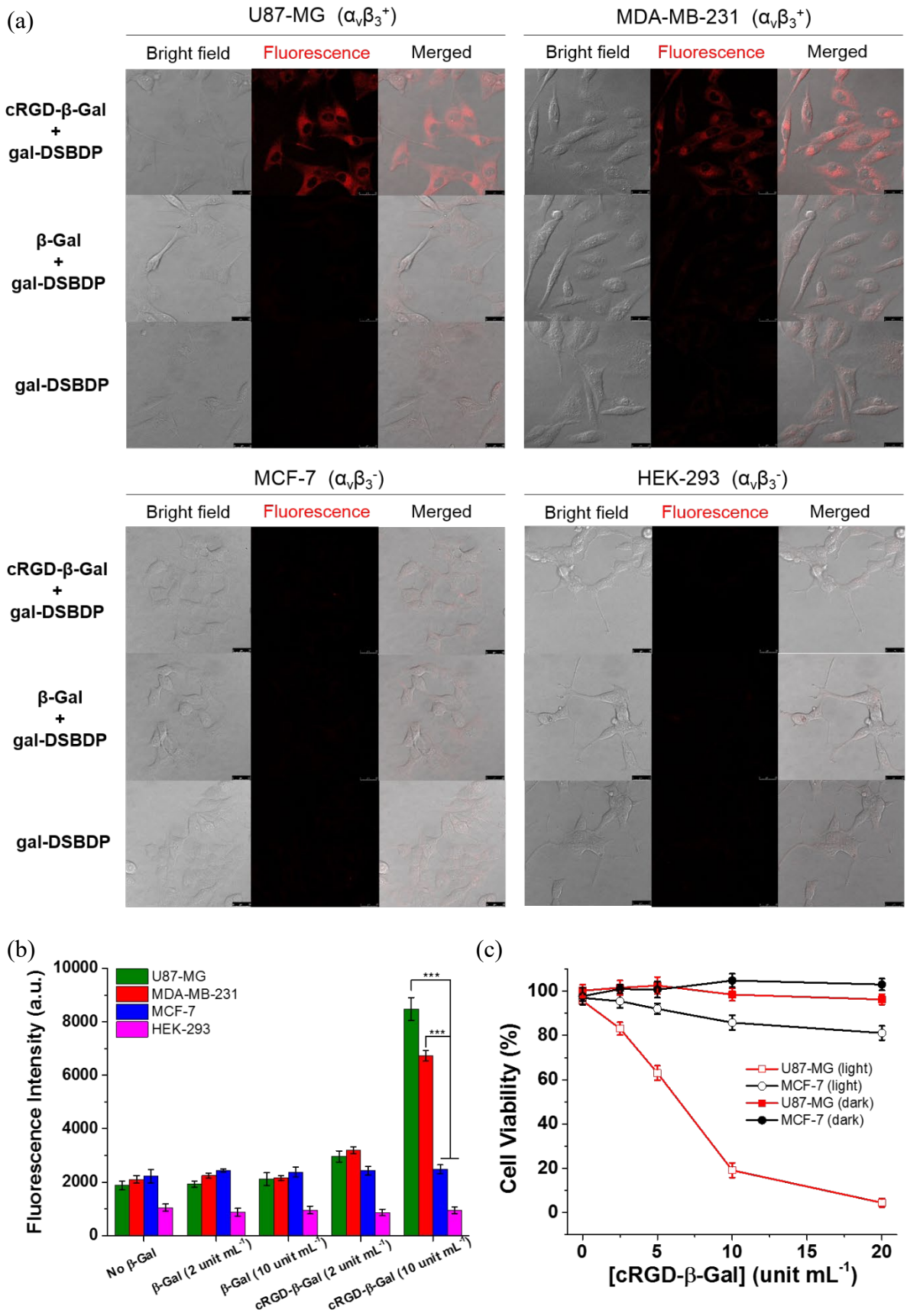
(a)
U87-MG (αvβ3+)
MDA-MB-231 (αvβ3+)
MCF-7 (αvβ3-)
HEK-293 (αvβ3-)
Bright field
Fluorescence
Merged
cRGD-β-Gal + gal-DSBDP
β-Gal + gal-DSBDP
gal-DSBDP
(b)
Fluorescence Intensity (a.u.)
U87-MG
MDA-MB-231
MCF-7
HEK-293
No β-Gal
β-Gal (2 unit mL-1)
β-Gal (10 unit mL-1)
cRGD-β-Gal (2 unit mL-1)
cRGD-β-Gal (10 unit mL-1)
***
(c)
Cell Viability (%)
U87-MG (light)
MCF-7 (light)
U87-MG (dark)
MCF-7 (dark)
[cRGD-β-Gal] (unit mL-1)

Figure 6. (a) Bright field, fluorescence, and the merged images of U87-MG, MDA-MB-231, MCF-7, and HEK-293 cells after incubation with **gal-DSBDP** (4 μM) for 30 min with or without preincubation with **cRGD-β-Gal** or β-Gal (10 unit mL^{-1}) for 1 h, followed by post-incubation in a drug-free medium for further 3 h. (b) Comparison of the intracellular fluorescence intensities in U87-MG, MDA-MB-231, MCF-7, and HEK-293 cells after incubation with **gal-DSBDP** (4 μM) for 30 min with or without preincubation with **cRGD-β-Gal** or β-Gal (2 and 10 unit mL^{-1}) for 1 h, followed by post-incubation in a drug-free medium for further 3 h. Data are expressed as the mean ± standard error of the mean (SEM) of three independent experiments. (c) Cell viability curves for U87-MG and MCF-7 cells with pre-treatment with different concentrations of **cRGD-β-Gal** for 1 h, followed by incubation with **gal-DSBDP** (4 μM) for 30 min and post-incubation for further 3 h, both in the absence and presence of light ($\lambda > 610$ nm, 23 mW cm^{-2}, 28 J cm^{-2}). Data are expressed as the mean ± SEM of three independent experiments, each performed in quadruplicate. ***$p < 0.001$ as calculated by the Student's t-test.

In Vivo Studies. To further investigate the bioorthogonal activation of **gal-DSBDP** by **cRGD-β-Gal** in vivo, U87-MG xenografted nude mice were treated with an intravenous injection of **cRGD-β-Gal** (10 unit mL^{-1} in PBS, 200 μL), native β-Gal (10 unit mL^{-1} in PBS, 200 μL), or PBS (200 μL). The latter two were used as the negative control. After 30 min, the activatable photosensitizer **gal-DSBDP** (1 mM, 20 μL) was injected intratumorally. The whole-body fluorescence images of the mice were then monitored continuously over 24 h and the fluorescence intensity per unit area of the tumor at different time points was also determined (Figure 7a). For the mice being administrated with the modified enzyme **cRGD-β-Gal**, the fluorescence intensity at the tumor grew along with time and reached the maximum at 6 h post-injection. At this time point, the intensity was approximately 3-fold and 12-fold higher than

that of the mice being injected with the native β-Gal and PBS, respectively. The selective lighting up of the fluorescence at the tumor site for this system could be attributed to the cyclic RGD-mediated uptake of **cRGD-β-Gal** by the integrin-positive U87-MG cells, followed by activation of **gal-DSBDP** therein through specific enzymatic cleavage. The small increase in fluorescence intensity for the mice being treated with native β-Gal might be due to the activation by the trace amount of β-Gal accumulated at the tumor during blood circulation. For the PBS control group, the fluorescence intensity was almost invisible throughout the 24 h, indicating that the photosensitizer could not be activated in the intrinsic tumor microenvironment. These results showed that the fluorescence emission of **gal-DSBDP** could also be activated selectively by the extrinsic **cRGD-β-Gal** with reduced background signal in an animal model.

The PDT efficacy of this extrinsic enzyme-activated photosensitizing system was then investigated. When the tumor size reached ca. 80-100 mm^3, the U87-MG tumor-bearing nude mice were injected with **cRGD-β-Gal** (10 unit mL^{-1} in PBS, 200 μL), native β-Gal (10 unit mL^{-1} in PBS, 200 μL), or PBS (200 μL) through the tail vein. After 30 min, a solution of **gal-DSBDP** in PBS (1 mM, 20 μL) was injected intratumorally. At 24 h post-injection, the tumor was illuminated with a diode laser for 10 min (λ = 680 nm, 0.1 W cm^{-2}, 60 J cm^{-2}). As another negative control, the mice were simply injected with PBS intravenously without further injection of **gal-DSBDP** and without the light treatment. After all these treatments, the tumor size was monitored continuously for 14 days. As shown in Figure 7b and 7c, upon injection of both **cRGD-β-Gal** and **gal-DSBDP** followed by laser irradiation, the tumor growth was greatly inhibited due to the bioorthogonal activation of the photodynamic activity of **gal-DSBDP** by **cRGD-β-Gal** inside the tumor. For the mice being treated with the native β-Gal, the tumor growth could be slightly retarded probably due to the activation by residual β-Gal as mentioned above. For the control group with injection of PBS and **gal-DSBDP** followed by light

irradiation, the tumor-inhibition effect was negligible as compared with the effect for injection of PBS alone. In addition, the body weight of the mice was also monitored during all these treatments. As shown in Figure 7d, there was no noticeable change during the course, suggesting that these treatments exerted no distinct side effect on the mice.

To further investigate the pathological changes after the treatment with this photosensitizing system, the tumor and major organs, including heart, liver, spleen, lung, and kidney of the mice were harvested on Day 14 after the PDT treatment for hematoxylin and eosin (H&E) histology analysis. For comparison, H&E staining was also performed for the other three control groups. As shown in Figure S8 in the Supporting Information, only the tumor from the mice receiving the PDT treatment of **cRGD-β-Gal** and **gal-DSBDP** showed significant cellular damage and more necrotic and apoptotic cells. These changes were not observed in the other three control groups. In addition, it was found that after this bioorthogonal PDT treatment, there was no major abnormality in the stained major organ slides, showing the minimal toxicity induced by this treatment.

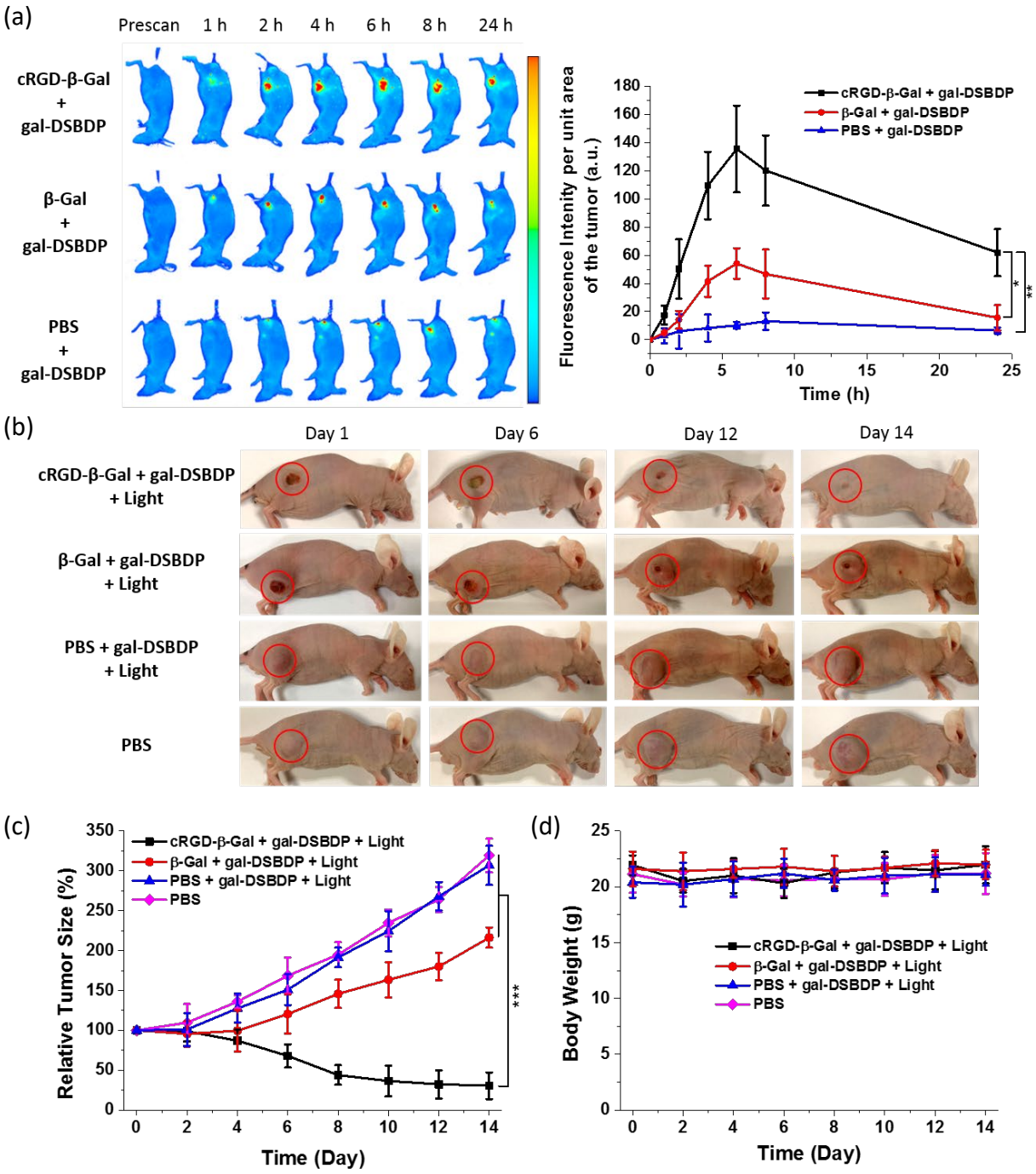

Figure 7. (a) Fluorescence images of U87-MG tumor-bearing nude mice and the quantified fluorescence intensity at the tumor before and after the intravenous injection of **cRGD-β-Gal** (10 unit mL^{-1} in PBS, 200 μL), native β-Gal (10 unit mL^{-1} in PBS, 200 μL), or PBS (200 μL), followed by the intratumoral injection of **gal-DSBDP** (1 mM, 20 μL) over a period of 24 h. (b) Photographs of U87-MG tumor-bearing nude mice after the above treatment and light irradiation (λ = 680 nm, 0.1 W cm^{-2}, 60 J cm^{-2}) at 24 h post-injection or the treatment with PBS

alone. (c) The corresponding tumor-growth curves over a period of 14 days. (d) Body weights of the mice after receiving the above treatments over a period of 14 days. Data are expressed as the mean value ± standard deviation of four independent experiments. *$p < 0.05$; **$p < 0.01$; ***$p < 0.001$ as calculated by the Student's t-test.

CONCLUSION

In summary, we have developed a novel and efficient approach for protein modification and delivery into cancer cells which involves the use of a bifunctional linker containing a bis(bromomethyl)phenyl group and an *o*-phthalaldehyde moiety to facilitate peptide cyclization through site-specific dibenzylation and protein conjugation via the PAC reaction, respectively. The modified GFP and β-Gal did not show any sign of denaturation and their native functions were retained after the modification. The β-Gal modified with cyclic RGD moieties **cRGD-β-Gal** could be selectively taken up by the $\alpha_v\beta_3$ integrin-positive U87-MG and MDA-MB-231 cells and activate **gal-DSBDP** therein through specific cleavage of the β-galactosidic bond followed by self-immolation. This "ester-to-carboxylate" conversion led to restoration of the photodynamic activities and cell eradication effectively. The bi orthogonal activation of **gal-DSBDP** using this extrinsic enzyme has also been demonstrated in vivo using U87-MG tumor-bearing nude mice. The activation effects, both in terms of the intratumoral fluorescence intensity and inhibition of the tumor growth, were significantly stronger than those by using the native β-Gal. Unlike the conventional design of enzyme-activated photosensitizers which depends on the difference in the expression level of intrinsic enzymes in the cancer cells and normal cells, the present approach involves selective delivery of an extrinsic enzyme into the target cancer cells for biorthogonal activation of a photosensitizer. It could largely reduce the off-target signals and improve the tumor specificity, leading to

enhanced treatment efficacy. Apart from PDT, it is envisaged that this approach can be applied readily for targeted delivery and activation or release of other theranostic agents.

ASSOCIATED CONTENT

Supporting Information

The Supporting Information is available free of charge at https://pubs.acs.org/doi/10.1021/jacs.

Experimental details; HPLC chromatograms and MALDI-TOF mass spectra of **cEBP-OPA** and **cRGD-OPA**; SDS-PAGE for **cEBP-GFP and cRGD-β-Gal**; UV-Vis and fluorescence spectra of **gal-DSBDP** and **9**; comparison of the enzymatic activity of **cRGD-β-Gal** and β-Gal; HPLC and ESI mass spectrometric analysis of the enzymatic reaction of **gal-DSBDP** and β-Gal; H&E staining for the tumor and main organs of the mice after the PDT treatment; NMR and mass spectra of all the new compounds (PDF)

AUTHOR INFORMATION

Corresponding Authors

Clarence T. T. Wong – *Department of Applied Biology and Chemical Technology and the State Key Laboratory of Chemical Biology and Drug Discovery, The Hong Kong Polytechnic University, Hung Hom, Hong Kong, China;* orcid.org/0000-0001-8950-0033; E-mail: clarence-tt.wong@polyu.edu.hk

Dennis K. P. Ng – *Department of Chemistry, The Chinese University of Hong Kong, Shatin, N.T., Hong Kong, China;* orcid.org/0000-0001-9087-960X; E-mail: dkpn@cuhk.edu.hk

Authors

Junlong Xiong – *Department of Chemistry, The Chinese University of Hong Kong, Shatin, N.T., Hong Kong, China*

Jacky C. H. Chu – *Department of Chemistry, The Chinese University of Hong Kong, Shatin, N.T., Hong Kong, China;* orcid.org/*0000-0003-3858-3312*

Wing-Ping Fong – *School of Life Sciences, The Chinese University of Hong Kong, Shatin, N.T., Hong Kong, China;* orcid.org/*0000-0002-0468-9883*

Author Contributions

J.X. and J.C.H.C. contributed equally.

Notes

The authors declare no competing financial interest.

ACKNOWLEDGMENTS

This work was supported by a General Research Fund from the Research Grants Council of the Hong Kong Special Administrative Region, China (Project No. 14303619).

REFERENCES

(1) Brown, S. B.; Brown, E. A.; Walker, I. The present and future role of photodynamic therapy in cancer treatment. *Lancet Oncol.* **2004**, *5*, 497−508.

(2) Correia, J. H.; Rodrigues, J. A.; Pimenta, S.; Dong, T.; Yang, Z. Photodynamic therapy review: principles, photosensitizers, applications, and future directions. *Pharmaceutics* **2021**, *13*, 1332.

(3) Algorri, J. F.; Ochoa, M.; Roldán-Varona, P.; Rodríguez-Cobo, L.; López-Higuera, J. M. Photodynamic therapy: a compendium of latest reviews. *Cancers* **2021**, *13*, 4447.

(4) Lan, M.; Zhao, S.; Liu, W.; Lee, C.-S.; Zhang, W.; Wang, P. Photosensitizers for photodynamic therapy. *Adv. Healthcare Mater.* **2019**, *8*, 1900132.

(5) Zhao, X.; Liu, J.; Fan, J.; Chao, H.; Peng, X. Recent progress in photosensitizers for overcoming the challenges of photodynamic therapy: from molecular design to application. *Chem. Soc. Rev.* **2021**, *50*, 4185−4219.

(6) Pham, T. C.; Nguyen, V.-N.; Choi, Y.; Lee, S.; Yoon, J. Recent strategies to develop innovative photosensitizers for enhanced photodynamic therapy. *Chem. Rev.* **2021**, *121*, 13454−13619.

(7) Sandland, J.; Boyle, R. W. Photosensitizer antibody-drug conjugates: past, present, and future. *Bioconjugate Chem.* **2019**, *30*, 975−993.

(8) Gierlich, P.; Mata, A. I.; Donohoe, C.; Brito, R. M. M.; Senge, M. O.; Gomes-da-Silva, L. C. Ligand-targeted delivery of photosensitizers for cancer treatment. *Molecules* **2020**, *25*, 5317.

(9) Luby, B. M.; Walsh, C. D.; Zheng, G. Advanced photosensitizer activation strategies for smarter photodynamic therapy beacons. *Angew. Chem. Int. Ed.* **2019**, *58*, 2558−2569.

(10) Cheng, P.; Pu, K. Activatable phototheranostic materials for imaging-guide cancer therapy. *ACS Appl. Mater. Interfaces* **2020**, *12*, 5286−5299.

(11) Yang, M.; Li, X.; Yoon, J. Activatable supramolecular photosensitizers: advanced design strategies. *Mater. Chem. Front.* **2021**, *5*, 1683−1693.

(12) Yao, C.; Li, Y.; Wang, Z.; Song, C.; Hu, X.; Liu, S. Cytosolic NQO1 enzyme-activated near-infrared fluorescence imaging and photodynamic therapy with polymeric vesicles. *ACS Nano* **2020,** *14*, 1919−1935.

(13) Palming, J.; Sjöholm, K.; Jernås, M.; Lystig, T. C.; Gummesson, A.; Romeo, S.; Lönn, L.; Lönn, M.; Carlsson, B.; Carlsson, L. M. S. The expression of NAD(P)H:quinone oxidoreductase 1 is high in human adipose tissue, reduced by weight loss, and correlates with adiposity, insulin sensitivity, and markers of liver dysfunction. *J. Clin. Endocrinol. Metab.* **2007,** *92*, 2346−2352.

(14) Zheng, G.; Chen, J.; Stefflova, K.; Jarvi, M.; Li, H.; Wilson, B. C. Photodynamic molecular beacon as an activatable photosensitizer based on protease-controlled singlet oxygen quenching and activation. *Proc. Natl. Acad. Sci. U. S. A.* **2007**, *104*, 8989−8994.

(15) Hu, C.; He, X.; Chen, Y.; Yang, X.; Qin, L.; Lei, T.; Zhou, Y.; Gong, T.; Huang, Y.; Gao, H. Metformin mediated PD-L1 downregulation in combination with photodynamic-immunotherapy for treatment of breast cancer. *Adv. Funct. Mater.* **2021**, *31*, 2007149.

(16) Kuivanen, T. T.; Jeskanen, L.; Kyllönen, L.; Impola, U.; Saarialho-Kere, U. K. Transformation-specific matrix metalloproteinases, MMP-7 and MMP-13, are present in epithelial cells of keratoacanthomas. *Mod. Pathol.* **2006,** *19*, 1203−1212.

(17) Wang, Y.; Jiang, L.; Zhang, Y.; Lu, Y.; Li, J.; Wang, H.; Yao, D.; Wang, D. Fibronectin-targeting and cathepsin B-activatable theranostic nanoprobe for MR/fluorescence imaging and enhanced photodynamic therapy for triple negative breast cancer. *ACS Appl. Mater. Interfaces* **2020**, *12*, 33564−33574.

(18) Tam, L. K. B.; Yu, L.; Wong, R. C. H.; Fong, W.-P.; Ng, D. K. P.; Lo, P.-C. Dual cathepsin B and glutathione-activated dimeric and trimeric phthalocyanine-based photodynamic molecular beacons for targeted photodynamic therapy. *J. Med. Chem.* **2021**, *64*, 17455−17467.

(19) Gondi, C. S.; Rao, J. S. Cathepsin B as a cancer target. *Expert Opin. Ther. Targets* **2013**, *17*, 281−291.

(20) Lozano-Torres, B.; Estepa-Fernández, A.; Rovira, M.; Orzáez, M.; Serrano, M.; Martínez-Máñez, R.; Sancenón, F. The chemistry of senescence. *Nat. Rev. Chem.* **2019**, *3*, 426−441.

(21) Yao, Y.; Zhang, Y.; Yan, C.; Zhu, W.-H.; Guo, Z. Enzyme-activatable fluorescent probes for β-galactosidase: from design to biological applications. *Chem. Sci.* **2021**, *12*, 9885−9894.

(22) Li, M.; Yang, M.; Zhu, W.-H. Advances in fluorescent sensors for β-galactosidase. *Mater. Chem. Front.* **2021**, *5*, 763−774.

(23) Chen, H.; Niu, G.; Wu, H.; Chen, X. Clinical application of radiolabeled RGD peptides for PET imaging of integrin $\alpha_v\beta_3$. *Theranostics* **2016**, *6*, 78−92.

(24) Chu, J. C. H.; Yang, C.; Fong, W.-P.; Wong, C. T. T.; Ng, D. K. P. Facile one-pot synthesis of cyclic peptide-conjugated photosensitisers for targeted photodynamic therapy. *Chem. Commun.* **2020**, *56*, 11941−11944.

(25) Chu, J. C. H.; Fong, W.-P.; Wong, C. T. T.; Ng, D. K. P. Facile synthesis of cyclic peptide-phthalocyanine conjugates for epidermal growth factor receptor-targeted photodynamic therapy. *J. Med. Chem.* **2021**, *64*, 2064−2076.

(26) Chu, J. C. H.; Chin, M. L.; Wong, C. T. T.; Hui, M.; Lo, P.-C.; Ng, D. K. P. One-pot synthesis of a cyclic antimicrobial peptide-conjugated phthalocyanine for synergistic chemo-photodynamic killing of multidrug-resistant bacteria. *Adv. Therap.* **2021**, *4*, 2000204.

(27) Wong, C. T. T.; Chu, J. C. H.; Ha, S. Y. Y.; Wong, R. C. H.; Dai, G.; Kwong, T.-T.; Wong, C.-H.; Ng, D. K. P. Phthalaldehyde-amine capture reactions for bioconjugation and immobilization of phthalocyanines. *Org. Lett.* **2020**, *22*, 7098−7102.

(28) Chu, J. C. H.; Shao, C.; Ha, S. Y. Y.; Fong, W.-P.; Wong, C. T. T.; Ng, D. K. P. One-pot peptide cyclisation and surface modification of photosensitiser-loaded red blood cells for targeted photodynamic therapy. *Biomater. Sci.* **2021**, *9*, 7832−7837.

(29) Chiper, M.; Niederreither, K.; Zuber, G. Transduction methods for cytosolic delivery of proteins and bioconjugates into living cells. *Adv. Healthcare Mater.* **2018**, *7*, 1701040.

(30) Scaletti, F.; Hardie, J.; Lee, Y.-W.; Luther, D. C.; Ray, M.; Rotello, V. M. Protein delivery into cells using inorganic nanoparticles-protein supramolecular assemblies. *Chem. Soc. Rev.* **2018**, *47*, 3421−3432.

(31) Lee, Y.-W.; Luther, D. C.; Kretzmann, J. A.; Burden, A.; Jeon, T.; Zhai, S.; Rotello, V. M. Protein delivery into the cell cytosol using non-viral nanocarriers. *Theranostics* **2019**, *9*, 3280−3292.

(32) Li, J.; Tuma, J.; Han, H.; Kim, H.; Wilson, R. C.; Lee, H. Y.; Murthy, N. The coiled-coil forming peptide $(KVSALKE)_5$ is a cell penetrating peptide that enhances the intracellular delivery of proteins. *Adv. Healthcare Mater.* **2021**, *10*, 2102118.

(33) Nischan, N.; Herce, H. D.; Natale, F.; Bohlke, N.; Budisa, N.; Cardoso, M. C.; Hackenberger, C. P. R. Covalent attachment of cyclic TAT peptides to GFP results in protein delivery into live cells with immediate bioavailability. *Angew Chem. Int. Ed.* **2015**, *54*, 1950−1953.

(34) Kitagishi, H.; Jiromaru, M.; Hasegawa, N. Intracellular delivery of adamantane-tagged small molecule, proteins, and liposomes using an octaarginine-conjugated β-cyclodextrin. *ACS Appl. Bio Mater.* **2020**, *3*, 4902−4911.

(35) Chiba, M.; Kamiya, M.; Tsuda-Sakurai, K.; Fujisawa, Y.; Kosakamoto, H.; Kojima, R.; Miura, M.; Urano, Y. Activatable photosensitizer for targeted ablation of *lac*Z-positive cells with single-cell resolution. *ACS Cent. Sci.* **2019**, *5*, 1676−1681.

(36) Zhou, Y.; Wong, R. C. H.; Dai, G.; Ng, D. K.P. A bioorthogonally activatable photosensitiser for site-specific photodynamic therapy. *Chem. Commun.* **2020**, *56*, 1078−1081.

(37) Xue, E. Y.; Shi, W.-J.; Fong, W.-P.; Ng, D. K. P. Targeted delivery and site-specific activation of β-cyclodextrin-conjugated photosensitizers for photodynamic therapy through a supramolecular bio-orthogonal approach. *J. Med. Chem.* **2021**, *64*, 15461−15476.

(38) Dai, G.; Chu, J. C. H.; Chan, C. K. W.; Choi, C. H. J.; Ng, D. K. P. Reactive oxygen species-responsive polydopamine nanoparticles for targeted and synergistic chemo and photodynamic anticancer therapy. *Nanoscale* **2021**, *13*, 15899−15915.

(39) Sun, W.; Zhao, X.; Fan, J.; Du, J.; Peng, X. Boron dipyrromethene nano-photosensitizers for anticancer phototherapies. *Small* **2019**, *15*, 1804927.

(40) Hwang, B.; Kim, T.-I.; Kim, H.; Jeon, S.; Choi, Y.; Kim, Y. Ubiquinone-BODIPY nanoparticles for tumor redox-responsive fluorescence imaging and photodynamic activity. *J. Mater. Chem. B* **2021**, *9*, 824−831.

(41) Ma, F.; Fischer, M.; Han, Y.; Withers, S. G.; Feng, Y.; Yang, G.-Y. Substrate engineering enabling fluorescence droplet entrapment for IVC-FACS-based ultrahigh-throughput screening. *Anal. Chem.* **2016**, *88*, 8587−8595.

(42) Chen, H.; He, X.; Su, M.; Zhai, W.; Zhang, H.; Li, C. A general strategy toward highly fluorogenic bioprobes emitting across the visible spectrum. *J. Am. Chem. Soc.* **2017**, *139*, 10157−10163.

(43) Jung, H. S.; Han, J.; Shi, H.; Koo, S.; Singh, H.; Kim, H.-J.; Sessler, J. L.; Lee, J. Y.; Kim, J.-H.; Kim, J. S. Overcoming the limits of hypoxia in photodynamic therapy: a carbonic anhydrase IX-targeted approach. *J. Am. Chem. Soc.* **2017**, *139*, 7595−7602.

(44) Zhu, S.; Zhang, J.; Vegesna, G.; Luo, F.-T.; Green, S. A.; Liu, H. Highly water-soluble neutral BODIPY dyes with controllable fluorescence quantum yields. *Org. Lett.* **2011**, *13*, 438−441.

(45) Ha, S. Y. Y.; Wong, R. C. H.; Wong, C. T. T.; Ng, D. K. P. An integrin-targeting glutathione-activated zinc(II) phthalocyanine for dual targeted photodynamic therapy. *Eur. J. Med. Chem.* **2019**, *174*, 56−65.

(46) Su, M.; Li, S.; Zhang, H.; Zhang, J.; Chen, H.; Li, C. Nano-assemblies from J-aggregated dyes: a stimuli-responsive tool applicable to living systems. *J. Am. Chem. Soc.* **2019**, *141*, 402−413.

(47) Wang, Z.-W.; Su, D.; Li, X.-Q.; Cao, J.-J.; Yang, D.-C.; Liu, J.-Y. A H_2O_2-responsive boron dipyrromethene-based photosensitizer for imaging-guided photodynamic therapy. *Molecules* **2019**, *24*, 32.

Supporting Information

Specific Activation of Photosensitizer with Extrinsic Enzyme for Precisive Photodynamic Therapy

Junlong Xiong,[†,#] Jacky C. H. Chu,[†,#] Wing-Ping Fong,[‡] Clarence T. T. Wong,*[§] and Dennis K. P. Ng*[†]

[†] *Department of Chemistry, The Chinese University of Hong Kong, Shatin, N.T., Hong Kong, China*

[‡] *School of Life Sciences, The Chinese University of Hong Kong, Shatin, N.T., Hong Kong, China*

[§] *Department of Applied Biology and Chemical Technology and State Key Laboratory of Chemical Biology and Drug Discovery, The Hong Kong Polytechnic University, Hung Hom, Kowloon, Hong Kong, China*

[#] *These authors contributed equally to this work*

Contents

Experimental Section

General

N,*N*-Dimethylformamide (DMF), tetrahydrofuran (THF), and CH_2Cl_2 were dried using an INERT solvent drying system prior to use. Acetonitrile was of HPLC grade. All other solvents were of analytical grade and used as received without further purification. All the reactions were performed under an atmosphere of nitrogen and monitored by thin layer chromatography (TLC; Merck pre-coated silica gel 60 F254 plates). Chromatographic purification was performed on a silica gel (Macherey-Nagel, 230–400 mesh) column with the indicated eluent. Compounds **1**,[R1] **2**,[R2] **5**,[R3] and **7**[R4] were prepared according to the literature procedure.

^1H and $^{13}C\{^1H\}$ NMR spectra were recorded on a Bruker Avance III 500 spectrometer (^1H, 500 MHz; ^{13}C, 125.8 MHz) in deuterated solvents. Spectra were referenced internally by using the residual solvent {^1H, δ = 7.26 (for $CDCl_3$), δ = 3.31 (for CD_3OD), δ = 2.50 [for dimethylsulfoxide (DMSO)-d_6]} or solvent [^{13}C, δ = 77.2 (for $CDCl_3$), δ = 49.0 (for CD_3OD), δ = 39.5 (for DMSO-d_6)] resonances relative to $SiMe_4$. Electrospray ionization (ESI) mass spectra were recorded on a Thermo Finnigan MAT 95 XL mass spectrometer or a Bruker SolariX 9.4 Tesla FTICR mass spectrometer. Matrix-assisted laser-desorption/ionization time-of-flight (MALDI-TOF) mass spectra were recorded on a Bruker Daltonics Autoflex III spectrometer. UV-Vis and steady-state fluorescence spectra were taken on a Shimazu UV-1800 UV-Vis spectrophotometer and a Horiba FluoroMax-4 spectrofluorometer, respectively.

Reverse-phase HPLC separation was performed on a XBridge BEH300 C18 column (5 μm, 4.6 mm × 150 mm) at a flow rate of 1 mL min^{-1} for analytical purpose or on a XBridge BEH300 Prep C18 column (5 μm, 10 mm × 250 mm) at a flow rate of 3 mL min^{-1} for preparative purpose using a Waters system equipped with a Waters 1525 binary pump and a Waters 2998 photodiode array detector. The solvents used for HPLC analysis were of HPLC grade. The condition used for the analysis was set as follows: solvent A = 0.1% trifluoroacetic

acid (TFA) in acetonitrile and solvent B = 0.1% TFA in deionized water; gradient: 5% A + 95% B in the first 5 min, and then changed to 15% A + 85% B in 10 min, further changed to 100% A + 0% B in 30 min, maintained under this condition for 5 min, changed to 0% A + 100% B in 5 min, and finally maintained under this condition for further 5 min.

Preparation of EBP and RGD Peptides

EBP (AcNH-CMYIEALDRYAC-$CONH_2$) and **RGD** (AcNH-CRGDfC-$CONH_2$) peptides were synthesized manually using a modified 9-fluorenylmethoxycarbonyl (Fmoc) solid-phase peptide synthesis protocol using the commercially available *N*-α-Fmoc-protected amino acids as the substrates and the rink amide resin as the solid support. A solution of 20% piperidine in DMF was used to remove the Fmoc protecting group, and 1-[bis(dimethylamino)methylene]-1H-1,2,3-triazolo-[4,5-b]pyridinium 3-oxide hexafluorophosphate (HATU) was used as the carboxyl group activating agent. An excess of the Fmoc-protected amino acid (4 equiv.), HATU (4 equiv.), and *N*,*N*-diisopropylethylamine (8 equiv.) in DMF were used for each coupling at room temperature. For the *N*-terminal acetylation, a mixture of CH_2Cl_2/pyridine/acetic anhydride (2:1:1 v/v/v) was added and the mixture was stirred at room temperature for 30 min. After washing with DMF and CH_2Cl_2, the resin was treated with a solution containing 95% TFA, 2.5% triisopropylsilane, and 2.5% CH_2Cl_2 for 1 h to cleave the peptide from the resin and remove the protecting groups. The resin was removed by filtration and the filtrate was precipitated by the addition of diethyl ether. After centrifugation, the supernatant was removed. The solid was redissolved in DMSO and then the solution was precipitated again using diethyl ether. Lyophilization of the precipitated peptide afforded the crude peptide, which was purified by reverse-phase HPLC followed by lyophilization. For **EBP**: HRMS (MALDI-TOF): *m/z* calcd for $C_{64}H_{99}N_{16}O_{19}S_3$ $[M+H]^+$, 1491.6429; found, 1491.6347.

For **RGD**: HRMS (MALDI-TOF): *m/z* calcd for $C_{29}H_{45}N_{10}O_9S_2$ $[M+H]^+$, 741.2807; found, 741.2610.

Preparation of cEBP-OPA and cRGD-OPA

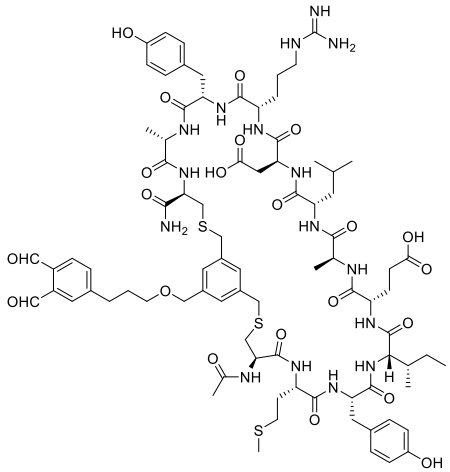

cEBP-OPA

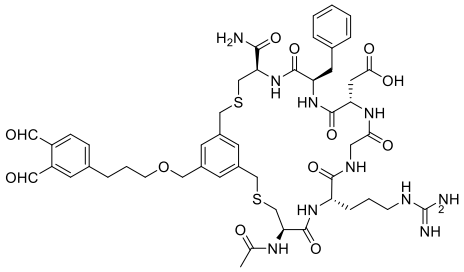

cRGD-OPA

Compound **1** was treated with a mixture of TFA and water (1:1 v/v) for 30 min at room temperature. After the in situ deprotection of the *ortho*-phthalaldehyde unit, the intermediate product was treated with **EBP** or **RGD** (1 mM) in borate buffer (pH 8.5) for 1 h at room temperature. Based on the HPLC analysis, the conversion for **cEBP-OPA** and **cRGD-OPA** was found to be 92% and 89%, respectively. For **cEBP-OPA**: HRMS (MALDI-TOF): *m/z* calcd for $C_{84}H_{117}N_{16}O_{22}S_3$ $[M+H]^+$, 1797.7685; found, 1797.7608. For **cRGD-OPA**: HRMS (MALDI-TOF): *m/z* calcd for $C_{49}H_{63}N_{10}O_{12}S_2$ $[M+H]^+$, 1047.4063; found, 1047.4093.

Preparation of Cyclic Peptide-Conjugated Proteins

Green fluorescent protein (GFP) or β-galactosidase (β-Gal) (lyophilized powder, Sigma) was first dissolved in phosphate-buffered saline (PBS) (pH 7.4) to afford a 5 μM stock solution. **cEBP-OPA** or **cRGD-OPA** was then added to the protein solution in PBS with a 20:1 mol ratio. The mixture was stirred at room temperature for 30 min and then filtrated through a molecular membrane filter (cut-off at 3 kDa) to remove the excess unconjugated peptide. The

modified proteins **cEBP-GFP** and **cRGD-β-Gal** were retained on the molecular membrane filter and re-dissolved in PBS for further use.

Preparation of 3

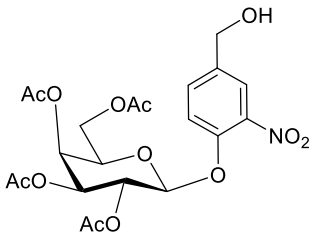

$NaBH_4$ (0.80 g, 21.1 mmol) was added to a solution of **2** (5.27 g, 10.6 mmol) in MeOH/CH_2Cl_2 (1:9 v/v, 40 mL) at 0 °C with stirring. The mixture was warmed to room temperature and stirred continuously for 2 h. The reaction was then quenched with 20% aqueous NH_4Cl (5 mL) and the mixture was extracted with ethyl acetate (100 mL). The organic layer was washed with saturated brine (30 mL), dried over anhydrous Na_2SO_4, filtered, and then evaporated under reduced pressure. The residue was purified by chromatography on a silica gel column using hexane/ethyl acetate (1:1 v/v) as the eluent to give **3** (3.97 g, 75%) as a white solid. ^{1}H NMR (500 MHz, $CDCl_3$): δ 7.79 (d, *J* = 2.0 Hz, 1 H, Ar-H), 7.51 (dd, *J* = 2.0, 8.5 Hz, 1 H, Ar-H), 7.33 (d, *J* = 8.5 Hz, 1 H, Ar-H), 5.52 (dd, *J* = 8.0, 10.5 Hz, 1 H, gal-H), 5.45 (d, *J* = 3.5 Hz, 1 H, gal-H), 5.09 (dd, *J* = 3.5, 10.5 Hz, 1 H, gal-H), 5.04 (d, *J* = 8.0 Hz, 1 H, gal-H), 4.71 (s, 2 H, $ArCH_2$), 4.25 (dd, *J* = 7.0, 11.5 Hz, 1 H, gal-H), 4.16 (dd, *J* = 6.0, 11.5 Hz, 1 H, gal-H), 4.05-4.08 (m, 1 H, gal-H), 2.18 (s, 3 H, OAc), 2.12 (s, 3 H, OAc), 2.06 (s, 3 H, OAc), 2.00 (s, 3 H, OAc). ^{13}C{^{1}H} NMR (125.8 MHz, $CDCl_3$): δ 170.5, 170.4, 170.3, 169.6, 148.5, 141.4, 137.3, 131.9, 123.3, 120.1, 101.0, 71.5, 70.7, 68.0, 66.9, 63.5, 61.5, 20.8 (2 overlapping signals), 20.7 (2 overlapping signals). HRMS (ESI): *m/z* calcd for $C_{21}H_{25}NNaO_{13}$ $[M+Na]^+$, 522.1218; found, 522.1217.

Preparation of 4

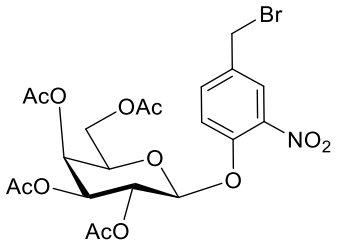

To a stirred solution of **3** (3.54 g, 7.1 mmol) in CH_2Cl_2 (40 mL) at 0 °C, a solution of PBr_3 (1.34 mL, 14.1 mmol) in CH_2Cl_2 (10 mL) was added dropwise via a dropping funnel. The mixture was warmed to room temperature and stirred for 4 h. The resulting mixture was diluted with CH_2Cl_2 (60 mL), which was then washed with saturated $NaHCO_3$ solution (20 mL × 3) and saturated brine (30 mL). The organic layer was dried over anhydrous Na_2SO_4, filtered, and then evaporated under reduced pressure. The residue was purified by chromatography on a silica gel column using hexane/ethyl acetate (4:1 v/v) as the eluent to afford **4** (2.87 g, 72%) as a colorless solid. ^{1}H NMR (500 MHz, $CDCl_3$): δ 7.80 (d, *J* = 3.0 Hz, 1 H, Ar-H), 7.53 (dd, *J* = 3.0, 11.0 Hz, 1 H, Ar-H), 7.31 (d, *J* = 11.0 Hz, 1 H, Ar-H), 5.50 (dd, *J* = 10.0, 13.0 Hz, 1 H, gal-H), 5.44 (d, *J* = 3.5 Hz, 1 H, gal-H), 5.07-5.10 (m, 2 H, gal-H), 4.44 (s, 2 H, $ArCH_2$), 4.22 (dd, *J* = 8.5, 14.0 Hz, 1 H, gal-H), 4.06-4.16 (m, 2 H, gal-H), 2.15 (s, 3 H, OAc), 2.08 (s, 3 H, OAc), 2.04 (s, 3 H, OAc), 1.98 (s, 3 H, OAc). $^{13}C\{^1H\}$ NMR (125.8 MHz, $CDCl_3$): δ 170.3, 170.2, 170.1, 169.4, 149.1, 141.0, 134.3, 133.8, 125.7, 119.9, 100.6, 71.5, 70.5, 67.8, 66.8, 61.4, 30.8, 20.7 (2 overlapping signals), 20.6 (2 overlapping signals). HRMS (ESI): *m/z* calcd for $C_{21}H_{24}BrNNaO_{12}$ $[M+Na]^+$, 586.0357; found, 586.0352.

Preparation of 6

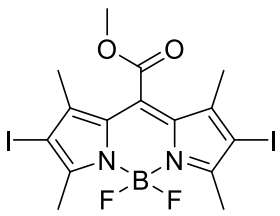

A mixture of **5** (0.64 g, 2.1 mmol) and *N*-iodosuccinimide (1.21 g, 5.4 mmol) in CH_2Cl_2 (50 mL) was stirred at room temperature for 6 h. After the consumption of **5** as indicated by TLC, the mixture was washed with saturated aqueous Na_2SO_3 (20 mL) and saturated brine (20 mL). The organic layer was dried over anhydrous Na_2SO_4, filtered, and then evaporated under reduced pressure. The residue was purified by chromatography on a silica gel column using hexane/ethyl acetate (5:1 v/v) as the eluent to give **6** (1.02 g, 86%) as a red solid. ^{1}H NMR (500 MHz, $CDCl_3$): δ 4.00 (s, 3 H, OCH_3), 2.62 (s, 6 H, CH_3), 2.13 (s, 6 H, CH_3). ^{13}C{^{1}H} NMR (125.8 MHz, $CDCl_3$): δ 165.4, 159.0, 143.6, 128.6, 128.4, 85.7, 53.6, 16.3, 15.2. HRMS (ESI): *m/z* calcd for $C_{15}H_{15}BF_2I_2N_2NaO_2$ $[M+Na]^+$, 580.9179; found, 580.9174.

Preparation of 8

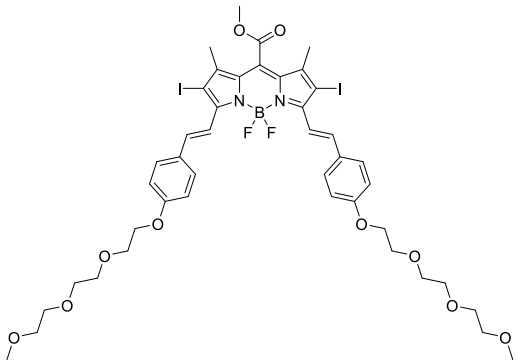

To a solution of benzaldehyde **7** (1.25 g, 4.7 mmol) in CH_3CN (40 mL), piperidine (0.80 mL) and acetic acid (0.80 mL) were added. The mixture was stirred at room temperature for 15 min, and then **6** (0.65 g, 1.2 mmol) was added. The resulting mixture was stirred under reflux with a small amount of dry molecular sieves added to remove the water produced. After the consumption of **6** as indicated by TLC, the mixture was cooled to room temperature and then filtered through a pad of Celite. The filtrate was evaporated in vacuo, and then the residue was purified by chromatography on a silica gel column with $CHCl_3$/MeOH (50:1 v/v) as the eluent to afford **8** (0.28 g, 23%) as a green solid. ^{1}H NMR (500 MHz, $CDCl_3$): δ 8.19 (d, *J* = 16.5 Hz, 2 H, C=CH), 7.59 (d, *J* = 9.0 Hz, 4 H, Ar-H), 7.54 (d, *J* = 16.5 Hz, 2 H, C=CH), 6.96 (d, *J* =

9.0 Hz, 4 H, Ar-H), 4.19 (t, *J* = 5.0 Hz, 4 H, OCH_2), 4.00 (s, 3 H, CO_2CH_3), 3.89 (t, *J* = 5.0 Hz, 4 H, OCH_2), 3.75-3.77 (m, 4 H, OCH_2), 3.69-3.71 (m, 4 H, OCH_2), 3.66-3.68 (m, 4 H, OCH_2), 3.55-3.57 (m, 4 H, OCH_2), 3.38 (s, 6 H, OCH_3), 2.20 (s, 6 H, CH_3). $^{13}C\{^1H\}$ NMR (125.8 MHz, $CDCl_3$): δ 166.0, 160.4, 151.8, 143.6, 140.2, 130.4, 129.6, 125.1, 116.7, 115.2, 82.7, 72.1, 71.0, 70.8, 70.7, 69.8, 67.7, 59.2, 53.5, 15.6. HRMS (ESI): *m/z* calcd for $C_{43}H_{51}BF_2I_2N_2NaO_{10}$ $[M+Na]^+$, 1081.1593; found, 1081.1589.

Preparation of 9

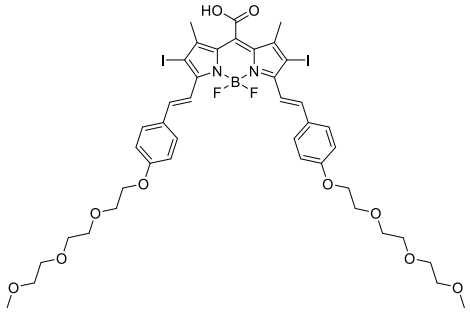

A mixture of **8** (0.21 g, 0.2 mmol) and LiI (0.27 g, 2.0 mmol) in ethyl acetate (30 mL) was stirred under reflux overnight. The mixture was cooled to room temperature and then washed with 0.1 M HCl (10 mL). The organic layer was dried over anhydrous Na_2SO_4 and then evaporated to dryness under reduced pressure. The residue was purified by chromatography on a silica gel column with $CHCl_3$/MeOH (20:1 v/v) as the eluent to afford **9** (0.18 g, 84%) as a green solid. ^1H NMR (500 MHz, CD_3OD): δ 8.15 (d, *J* = 17.0 Hz, 2 H, C=CH), 7.57 (d, *J* = 8.5 Hz, 4 H, Ar-H), 7.53 (d, *J* = 17.0 Hz, 2 H, C=CH), 7.02 (d, *J* = 8.5 Hz, 4 H, Ar-H), 4.17-4.19 (m, 4 H, OCH_2), 3.84-3.86 (m, 4 H, OCH_2), 3.69-3.72 (m, 4 H, OCH_2), 3.62-3.67 (m, 8 H, OCH_2), 3.52-3.54 (m, 4 H, OCH_2), 3.35 (s, 6 H, OCH_3), 2.48 (s, 6 H, CH_3). $^{13}C\{^1H\}$ NMR (125.8 MHz, CD_3OD): δ 171.2, 161.5, 150.9, 145.7, 139.3, 130.9, 130.6, 129.9, 117.9, 116.2, 81.1, 79.5, 73.0, 71.8, 71.6, 71.4, 70.8, 68.7, 59.1, 16.1. HRMS (ESI): *m/z* calcd for $C_{42}H_{49}BF_2I_2N_2NaO_{10}$ $[M+Na]^+$, 1067.1437; found, 1067.1448.

Preparation of 10

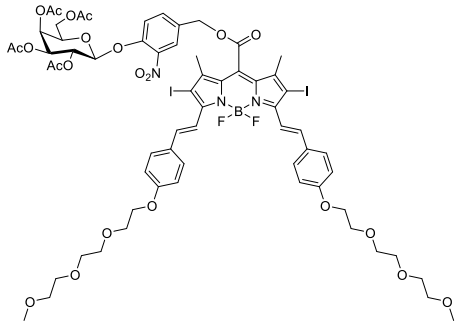

A mixture of **4** (270 mg, 0.48 mmol), **9** (125 mg, 0.12 mmol), and triethylamine (67 μL, 0.48 mmol) in THF (15 mL) was stirred at room temperature overnight. After removing the solvent in vacuo, the residue was purified by chromatography on a silica gel column using $CHCl_3$/MeOH (40:1 v/v) as the eluent to afford **10** (77 mg, 42%) as a green solid. ^{1}H NMR (500 MHz, $CDCl_3$): δ 8.19 (d, *J* = 16.5 Hz, 2 H, C=CH), 7.89 (d, *J* = 2.0 Hz, 1 H, Ar-H), 7.58-7.61 (m, 5 H, Ar-H), 7.53 (d, *J* = 16.5 Hz, 2 H, C=CH), 7.42 (d, *J* = 8.5 Hz, 1 H, Ar-H), 6.97 (d, *J* = 9.0 Hz, 4 H, Ar-H), 5.52-5.58 (m, 1 H, gal-H), 5.47-5.48 (m, 1 H, gal-H), 5.41 (s, 2 H, $ArCH_2$), 5.10-5.13 (m, 2 H, gal-H), 4.23-4.25 (m, 1 H, gal-H), 4.18-4.20 (m, 5 H, OCH_2 and gal-H), 4.07-4.09 (m, 1 H, gal-H), 3.88-3.90 (m, 4 H, OCH_2), 3.75-3.77 (m, 4 H, OCH_2), 3.68-3.70 (m, 4 H, OCH_2), 3.65-3.67 (m, 4 H, OCH_2), 3.54-3.56 (m, 4 H, OCH_2), 3.38 (s, 6 H, OCH_3), 2.19 (s, 3 H, OAc), 2.14 (s, 3 H, OAc), 2.11 (s, 6 H, CH_3), 2.07 (s, 3 H, OAc), 2.02 (s, 3 H, OAc). ^{13}C{^{1}H} NMR (125.8 MHz, $CDCl_3$): δ 170.4, 170.3, 170.2, 169.5, 165.2, 160.5, 152.0, 149.9, 143.3, 141.4, 140.5, 130.3, 129.9, 129.7, 129.6, 129.5, 129.3, 125.9, 124.2, 120.3, 116.6, 115.2, 115.1, 100.9, 82.9, 72.1, 71.7, 71.0, 70.8, 70.7, 70.6, 69.8, 67.9, 67.7, 67.0, 66.8, 61.4, 59.2, 20.9, 20.8, 20.7, 15.9. HRMS (ESI): *m/z* calcd for $C_{63}H_{72}BF_2I_2N_3NaO_{22}$ $[M+Na]^+$, 1548.2660; found, 1548.2653.

Preparation of gal-DSBDP

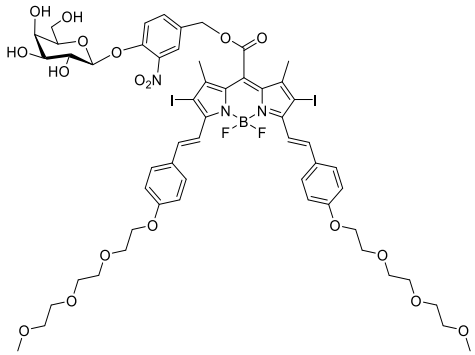

A mixture of **10** (61 mg, 0.04 mmol) and K_2CO_3 (17 mg, 0.12 mmol) in MeOH/$CHCl_3$ (1:4 v/v, 10 mL) was stirred at room temperature for 4 h. After the consumption of **10** as indicated by TLC, the solvent was evaporated under reduced pressure, and the residue was purified by chromatography on a silica gel column using $CHCl_3$/ MeOH (10:1 v/v) as the eluent to afford **gal-DSBDP** (44 mg, 80%) as a green solid. ^{1}H NMR (500 MHz, DMSO-d_6): δ 8.15 (d, *J* = 16.5 Hz, 2 H, C=CH), 8.10 (d, *J* = 2.0 Hz, 1 H, Ar-H), 7.81 (dd, *J* = 2.0, 9.0 Hz, 1 H, Ar-H), 7.59 (d, *J* = 8.5 Hz, 4 H, Ar-H), 7.48 (d, *J* = 9.0 Hz, 1 H, Ar-H), 7.38 (d, *J* = 16.5 Hz, 2 H, C=CH), 7.07 (d, *J* = 8.5 Hz, 4 H, Ar-H), 5.55 (s, 2 H, $ArCH_2$), 5.19 (d, *J* = 5.5 Hz, 1 H, gal-H), 5.09 (d, *J* = 7.5 Hz, 1 H, gal-H), 4.90 (d, *J* = 6.0 Hz, 1 H, gal-H), 4.66 (t, *J* = 5.5 Hz, 1 H, gal-H), 4.60 (d, *J* = 4.5 Hz, 1 H, gal-H), 4.15-4.17 (m, 4 H, OCH_2), 3.75-3.77 (m, 4 H, OCH_2), 3.69-3.73 (m, 1 H, gal-H), 3.64-3.68 (m, 1 H, gal-H), 3.57-3.60 (m, 4 H, OCH_2), 3.50-3.55 (m, 8 H, OCH_2), 3.41-3.43 (m, 4 H, OCH_2), 3.23 (s, 6 H, OCH_3), 2.13 (s, 6 H, CH_3). ^{13}C{^{1}H} NMR (125.8 MHz, DMSO-d_6): δ 164.3, 160.3, 151.5, 150.0, 143.7, 140.1, 140.0, 135.3, 129.6, 129.3, 128.8, 128.4, 127.2, 126.0, 124.5, 117.4, 115.7, 115.4, 115.3, 101.0, 84.8, 75.8, 73.3, 71.3, 70.0, 69.8, 69.6, 68.8, 67.9, 67.7, 67.5, 60.2, 58.1, 15.5. HRMS (ESI): *m/z* calcd for $C_{55}H_{64}BF_2I_2N_3NaO_{18}$ $[M+Na]^+$, 1380.2237; found, 1380.2237.

Determination of Fluorescence Quantum Yields

The fluorescence quantum yields (Φ_F) were determined by the equation:[R5]

$$\Phi_{F(sample)} = \left(\frac{F_{sample}}{F_{ref}}\right)\left(\frac{A_{ref}}{A_{sample}}\right)\left(\frac{n^2_{sample}}{n^2_{ref}}\right)\Phi_{F(ref)}$$

where *F*, *A*, and *n* are the measured fluorescence (area under the emission peak), the absorbance at the excitation wavelength (610 nm), and the refractive index of the solvent, respectively. The unsubstituted zinc(II) phthalocyanine (ZnPc) in DMF was used as the reference [$\Phi_{F(ref)}$ = 0.28].[R6] To minimize re-absorption of radiation by the ground-state species, the emission spectra were obtained in very dilute solutions of which the absorbance at the excitation wavelength was less than 0.05.

Measurement of Singlet Oxygen Generation

1,3-Diphenylisobenzofuran (DPBF) was used as the singlet oxygen scavenger. Compound **9** and **gal-DSBDP** (2 μM) were dissolved in PBS (pH 7.4) with 10% DMSO (v/v), respectively, and the solutions were left at 37 ^oC for 3 h with or without β-Gal (6 unit mL^{-1}) before DPBF (80 μM) was added. The resulting solutions were irradiated with red light from a 300 W halogen lamp after passing through a water tank for cooling and a color glass filter with a cut-on wavelength at 610 nm (Newport). The absorption maximum of DPBF at 417 nm was monitored along with the irradiation time.

Study of the Stability at Different pH and in Serum

For studying the stability of **gal-DSBDP** at different pH, the compound was dissolved in PBS with 10% DMSO (v/v) at different pH values (3, 5, 7.4, 9, and 11) at room temperature. These solutions were then subjected to HPLC analysis. For studying the stability of **gal-DSBDP** in serum, it was dissolved in Dulbecco's Modified Eagle Medium (DMEM) (ThermoFisher

Scientific, cat. no. 12100-046) with 20% fetal bovine serum (FBS) (ThermoFisher Scientific, cat. no. 10270-106) (v/v) and 10% DMSO (v/v) at 37 °C. An aliquot of the solution was drawn at different time points and precipitated with an equal volume of cold methanol. The mixture was centrifuged, and the supernatant was collected for HPLC analysis. The peak areas of **gal-DSBDP** at different time points were compared.

Cell Lines and Culture Conditions

A549 human lung carcinoma cells (ATCC, no. CCL-185) and HEK-293 human embryonic kidney cells (ATCC, no. CRL-1573) were maintained in DMEM supplemented with FBS (10%) and penicillin-streptomycin (100 unit mL^{-1} and 100 μg mL^{-1}, respectively). HT29 human colorectal adenocarcinoma cells (ATCC, no. HTB-38), HeLa human cervical carcinoma cells (ATCC, no. CCL-2), MDA-MB-231 human breast adenocarcinoma cells (ATCC, no. HTB-26), and MCF-7 human breast adenocarcinoma cells (ATCC, no. HTB-22) were maintained in Roswell Park Memorial Institute (RPMI) 1640 medium (Invitrogen, cat. no. 23400-021) supplemented with FBS (10%) and penicillin-streptomycin (100 unit mL^{-1} and 100 μg mL^{-1}, respectively). U87-MG human glioblastoma cells (ATCC, no. HTB-14) were maintained in Minimum Essential Medium (MEM) (Sigma-Aldrich, no. M5650) supplemented with FBS (10%) and penicillin-streptomycin (100 unit mL^{-1} and 100 μg mL^{-1}, respectively). All the cells were grown at 37 ^{o}C in a humidified 5% CO_2 atmosphere.

Confocal Fluorescence Microscopic Study

Approximately 2×10^5 cells in DMEM, RPMI 1640 medium, or MEM (2 mL) were seeded on a glass-bottom confocal dish and incubated overnight at 37 °C in a humidified 5% CO_2 atmosphere. For the study of GFP binding, the cells, after being rinsed with PBS, were incubated with **cEBP-GFP** or the native GFP (0.1 mM) in a serum-free medium at 37 °C for 1

h. For the study of the extrinsic enzyme-activated photosensitizing system, the cells, after being rinsed with PBS, were incubated with **cRGD-β-Gal** or the native β-Gal (10 unit mL^{-1}) in a serum-free medium at 37 °C for 1 h. After removing the medium, the cells were rinsed with PBS twice and then treated with **gal-DSBDP** (4 μM) in a serum-free medium at 37 °C for 30 min. The cells were rinsed with PBS twice, followed by post-incubation in a serum-free medium for further 3 h. The solution was then removed, and the cells were rinsed with PBS twice before being examined using a Leica TCS SP8 high speed confocal microscope equipped with solid-state 488 and 638 nm lasers. The GFP was excited at 488 nm and its fluorescence was monitored at 500−530nm. The photosensitizer was excited at 638 nm and its fluorescence was monitored at 650−750 nm. The images were digitized and analyzed using a Leica Application Suite X software.

Flow Cytometric Analysis

Approximately 2×10^5 cells per well in DMEM, RPMI 1640 medium, or MEM (2 mL) were seeded on a 6-multiwell plate and incubated overnight at 37 °C in a humidified 5% CO_2 atmosphere. After being rinsed with PBS, the cells were incubated with different concentrations of **cRGD-β-Gal** or the native β-Gal (0, 2, or 10 unit mL^{-1}) in a serum-free medium at 37 ºC for 1 h. After removing the medium, the cells were rinsed with PBS twice and then treated with **gal-DSBDP** (4 μM) in a serum-free medium at 37 °C for 30 min. The cells were then rinsed with PBS twice, followed by post-incubation in a serum-free medium for further 3 h. The solution was then removed, and the cells were rinsed with PBS twice and harvested by 0.25% trypsin-ethylenediaminetetraacetic acid (Invitrogen, 0.2 mL) for 5 min. The activity of trypsin was quenched with a serum-containing medium (0.5 mL), and the mixture was centrifuged at 1500 rpm for 3 min at room temperature. The pellet was washed with PBS (1.0 mL) and then subjected to centrifugation. The cells were then suspended in PBS

(1.0 mL) and the intracellular fluorescence intensities were measured using a BD FACSVerse flow cytometer (Becton Dickinson) with 10^4 cells counted in each sample. The photosensitizer was excited by an argon laser at 640 nm and the emitted fluorescence was monitored at 650−750 nm. The data collected were analyzed using the BD FACSuite. All experiments were performed in triplicate.

Study of Intracellular ROS Generation

Approximately 2×10^5 cells in DMEM, RPMI 1640 medium, or MEM (2 mL) were seeded on a glass-bottom confocal dish and incubated overnight at 37 °C in a humidified 5% CO_2 atmosphere. The cells, after being rinsed with PBS, were incubated with **cRGD-β-Gal** or the native β-Gal (10 unit mL^{-1}) in a serum-free medium at 37 °C for 1 h. After removing the medium, the cells were rinsed with PBS twice and then treated with **gal-DSBDP** (4 μM) in a serum-free medium at 37 °C for 30 min. The cells were rinsed with PBS twice, followed by incubation in a serum-free medium for further 3 h. The solution was then removed, and the cells were rinsed with PBS twice and then incubated with 2',7'-dichlorodihydrofluorescein diacetate (H_2DCFDA) in PBS (10 μM, 1 mL) at 37 °C for 30 min. The cells were rinsed and refilled with PBS before being illuminated at ambient temperature. The light source consisted of a 300 W halogen lamp, a water tank for cooling, and a color glass filter (Newport) cut-on at $\lambda = 610$ nm. The fluence rate ($\lambda > 610$ nm) was 23 mW cm^{-2}. Illumination of 10 min led to a total fluence of 14 J cm^{-2}. After illumination, the cells were examined with a Leica TCS SP8 high speed confocal microscope equipped with a 488 nm laser. The fluorescent product of the oxidation of H_2DCFDA by ROS, namely 2',7'-dichlorofluorescein (DCF), was excited at 488 nm and its fluorescence was monitored at 500−550 nm. The images were digitized and analyzed using a Leica Application Suite X software.

Photocytotoxicity Assay

Approximately 2×10^4 cells per well in DMEM, RPMI 1640 medium, or MEM (100 μL) were inoculated in 96-multiwell plates and incubated overnight at 37 ℃ in a humidified 5% CO_2 atmosphere. A stock solution of **gal-DSBDP** (1 mM) was prepared by dissolving the compound (40 nmol) in DMSO (40 μL). The solution was diluted with a serum-free medium to 4 μM. After being rinsed with PBS twice, the cells were pretreated with **cRGD-β-Gal** (100 μL for each well) at various concentrations (0, 2.5, 5, 10, or 20 unit mL^{-1}) for 1 h at 37 °C under 5% CO_2. After being rinsed with PBS twice, the cells were further incubated with **gal-DSBDP** (4 μM) in the dark for 30 min and then rinsed with PBS twice, followed by post-incubation in a culture medium (100 μL) for further 3 h before being illuminated at ambient temperature. The light source consisted of a 300 W halogen lamp, a water tank for cooling, and a color glass filter (Newport) cut-on at λ = 610 nm. The fluence rate (λ > 610 nm) was 23 mW cm^{-2}. Illumination of 20 min led to a total fluence of 28 J cm^{-2}. Cell viability was determined by means of a colorimetric 3-(4,5-dimethylthiazol-2-yl)-2,5-diphenyltetrazolium bromide (MTT) assay.[R7] After illumination, the cells were incubated at 37 °C under 5% CO_2 overnight. A MTT (Sigma) solution in PBS (3 mg mL^{-1}, 50 μL) was added to each well followed by incubation for 4 h under the same environment. DMSO (100 μL) was then added to each well. Solutions in all the wells were mixed until homogenous. The absorbance at 490 nm of each well on the plate was taken by a microplate reader (Tecan Spark 10M) at ambient temperature. The average absorbance of the blank wells, which did not contain the cells, was subtracted from the readings of the other wells. The cell viability was then determined by the equation:

$$\% \text{ viability} = \frac{\Sigma\left(\frac{A_\text{i}}{A_\text{control}}\right)\times 100}{n},$$

where A_i is the absorbance of the i^{th} datum (i = 1, 2, …, n), A_control is the average absorbance of the control wells in which the compound was absent, and n (=4) is the number of data points.

In Vivo Imaging

Female Balb/c nude mice (20–25 g) were obtained from the Laboratory Animal Services Centre at The Chinese University of Hong Kong. All animal experiments were approved by the Animal Experimentation Ethics Committee of the University. The mice were kept under a pathogen-free condition with free access to food and water. U87-MG cells (1×10^7 cells in 200 μL) were inoculated subcutaneously at the back of the mice. A stock solution (1 mM) of **gal-DSBDP** (200 nmol) was prepared by dissolving it in DMSO (15 μL) followed by dilution with distilled water (185 μL). Once the tumors had grown to a size of 80−100 mm^3, 200 μL of **cRGD-β-Gal** (10 unit mL^{-1}), β-Gal (10 unit mL^{-1}), or PBS was injected to the mice through the tail vein. After 30 min, the **gal-DSBDP** solution (20 μL) was injected intratumorally. The fluorescence image of the mice was captured before and after the injection at different time points up to 24 h using an Odyssey infrared imaging system (excitation wavelength = 680 nm, emission wavelength ≥ 700 nm). The images were digitized and analyzed by the Odyssey imaging system software (no. 9201-500). Four mice were used for each group.

In Vivo Photodynamic Therapy

U87-MG tumor-bearing nude mice were prepared as described above. The length and width of the tumor were measured by a micrometer digital caliper (SCITOP Systems). The tumor volume (mm^3) was calculated by the formula: tumor volume = (length × $width^2$)/2. A stock solution of **gal-DSBDP** (1 mM) was prepared as described above. Once the tumors had grown to a size of 80–100 mm^3, 200 μL of **cRGD-β-Gal** (10 unit mL^{-1}), β-Gal (10 unit mL^{-1}), or PBS was injected to the tumor-bearing mice through the tail vein. After 30 min, the **gal-DSBDP** solution (20 μL) was injected intratumorally. At 24 h post-injection, the tumor was illuminated by a diode laser (Biolitec Ceralas) at 680 nm operated at 0.08 W. Illumination on a circular spot with 1.0 cm diameter for 10 min led to a total fluence of 60 J cm^{-2}. Another set of control

experiment was performed by injecting PBS alone without **gal-DSBDP** and light irradiation. The tumor size of the nude mice was monitored periodically for the next 14 days. The tumor volumes were compared with those for the PBS control group without other treatments. Four mice were used for each group. On Day 14 after the PDT treatment, the mice were sacrificed, and the major organs and tumors were harvested. The tissues were fixed with 4% paraformaldehyde, dehydrated in an alcohol series, mixed with solutions of xylene and paraffin, and then embedded in paraffin. The tissue sections were prepared by a Leica RM2235 microtome. After staining with hematoxylin and eosin (H&E), the tissues were examined with a Carl Zeiss PALM inverted microscope. Four mice were used for each group.

Statistical Analysis

Data shown on the figures are presented as the mean ± standard error of the mean (SEM) or standard deviation (SD). The data were analyzed using Student's t-test with p values < 0.05 considered as significant; *p < 0.05; **p < 0.01; ***p < 0.001. Statistical calculations were performed using Microsoft Excel (Microsoft Corporation, Redmond, WA, USA).

References

(R1) Chu, J. C. H.; Shao, C.; Ha, S. Y. Y.; Fong, W.-P.; Wong, C. T. T.; Ng, D. K. P. One-pot peptide cyclisation and surface modification of photosensitiser-loaded red blood cells for targeted photodynamic therapy. *Biomater. Sci.* **2021**, *9*, 7832−7837.

(R2) Ma, F.; Fischer, M.; Han, Y.; Withers, S. G.; Feng, Y.; Yang, G.-Y. Substrate engineering enabling fluorescence droplet entrapment for IVC-FACS-based ultrahigh-throughput screening. *Anal. Chem.* **2016**, *88*, 8587−8595.

(R3) Chen, H.; He, X.; Su, M.; Zhai, W.; Zhang, H.; Li, C. A general strategy toward highly fluorogenic bioprobes emitting across the visible spectrum. *J. Am. Chem. Soc.* **2017**, *139*, 10157−10163.

(R4) Jung, H. S.; Han, J.; Shi, H.; Koo, S.; Singh, H.; Kim, H.-J.; Sessler, J. L.; Lee, J. Y.; Kim, J.-H.; Kim, J. S. Overcoming the limits of hypoxia in photodynamic therapy: a carbonic anhydrase IX-targeted approach. *J. Am. Chem. Soc.* **2017**, *139*, 7595−7602.

(R5) Eaton, D. F. Reference materials for fluorescence measurement. *Pure Appl. Chem.* **1988**, *60*, 1107−1114.

(R6) Scalise, I.; Durantini, E. N. Synthesis, properties, and photodynamic inactivation of Escherichia coli using a cationic and a noncharged Zn(II) pyridyloxyphthalocyanine derivatives. *Bioorg. Med. Chem*. **2005**, *13*, 3037−3045.

(R7) Tada, H.; Shiho, O.; Kuroshima, K.-i.; Koyama, M.; Tsukamoto, K. An improved colorimetric assay for interleukin 2. *J. Immunol. Methods* **1986**, *93*, 157−165.

Table S1. Electronic absorption and fluorescence data for **gal-DSBDP** and **9** in PBS (pH 7.4) with 10% DMSO (v/v).

Compound	λ_{abs} (nm) (log ε)	λ_{em} (nm)[a]	Φ_F[b]
gal-DSBDP	329 (4.33), 397 (4.34), 473 (4.09), 655 (4.52), 710 (4.56)	735	0.01
9	371 (4.69), 430 (4.12), 610 (shoulder), 651 (4.83)	685	0.14

[a] Excited at 610 nm. [b] Using ZnPc as the reference (Φ_F = 0.28 in DMF).

(a)

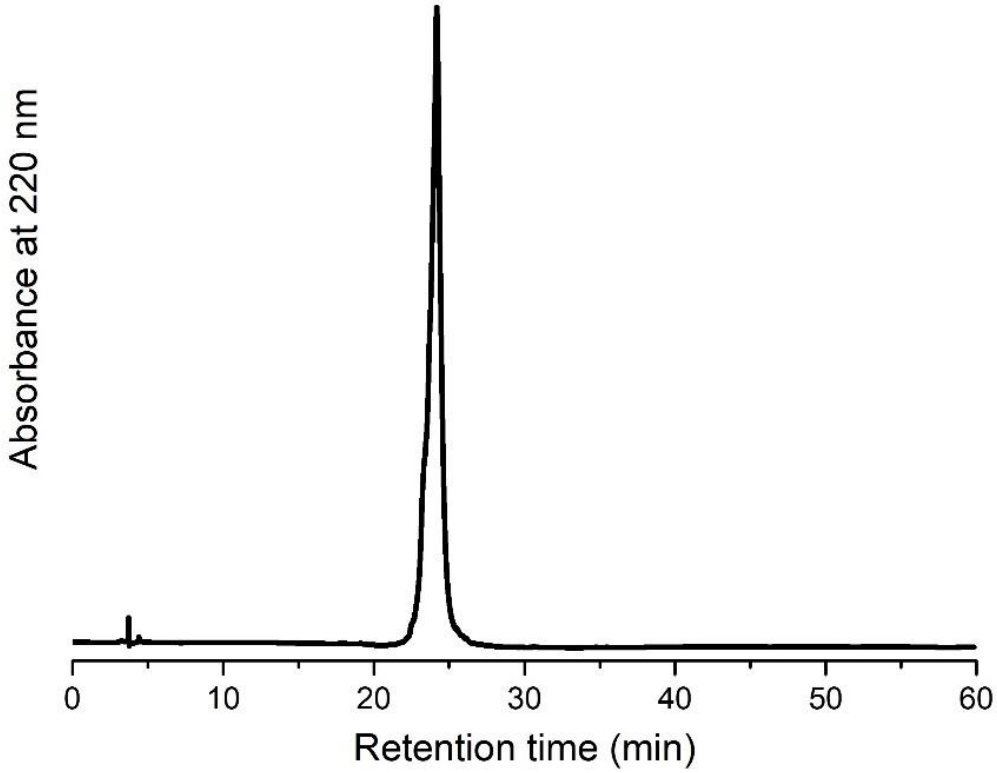

(b)

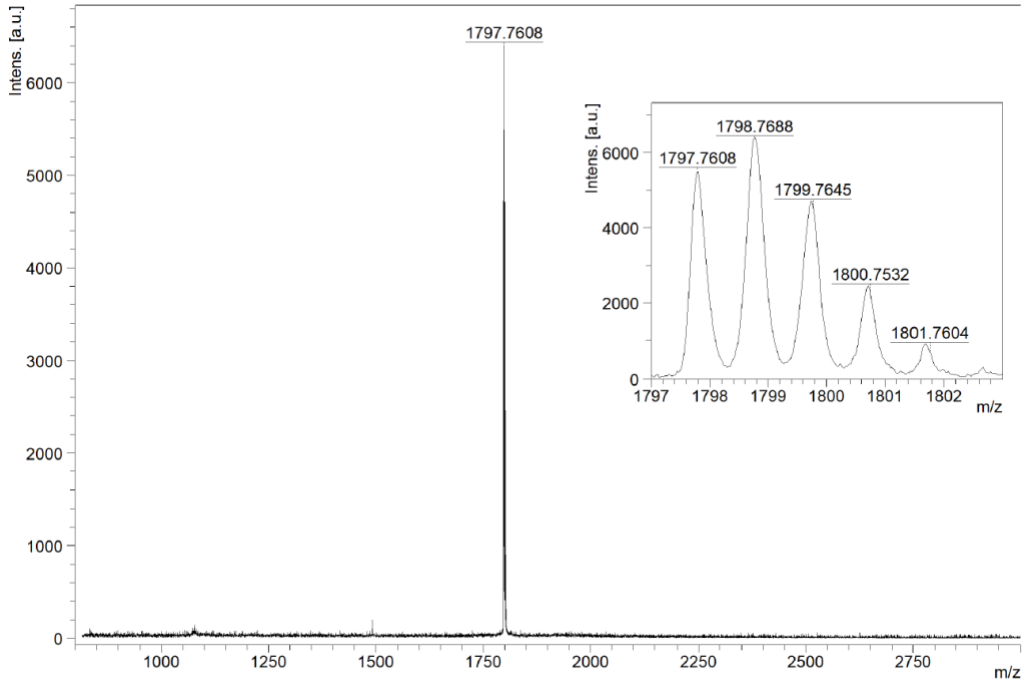

Figure S1. (a) HPLC chromatogram and (b) MALDI-TOF mass spectrum of **cEBP-OPA**.

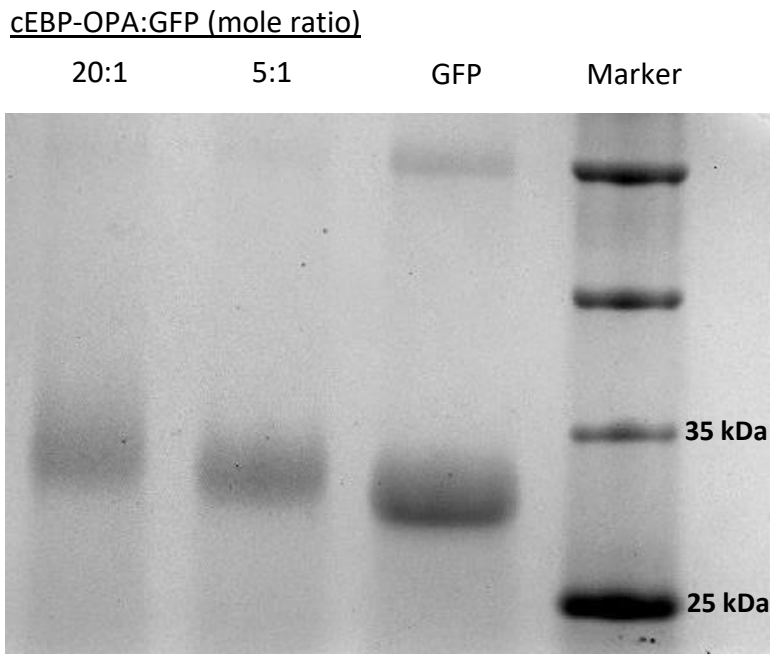

Figure S2. SDS-PAGE analysis of the native GFP and GFP conjugated with different mole ratios of **cEBP-OPA**.

(a)

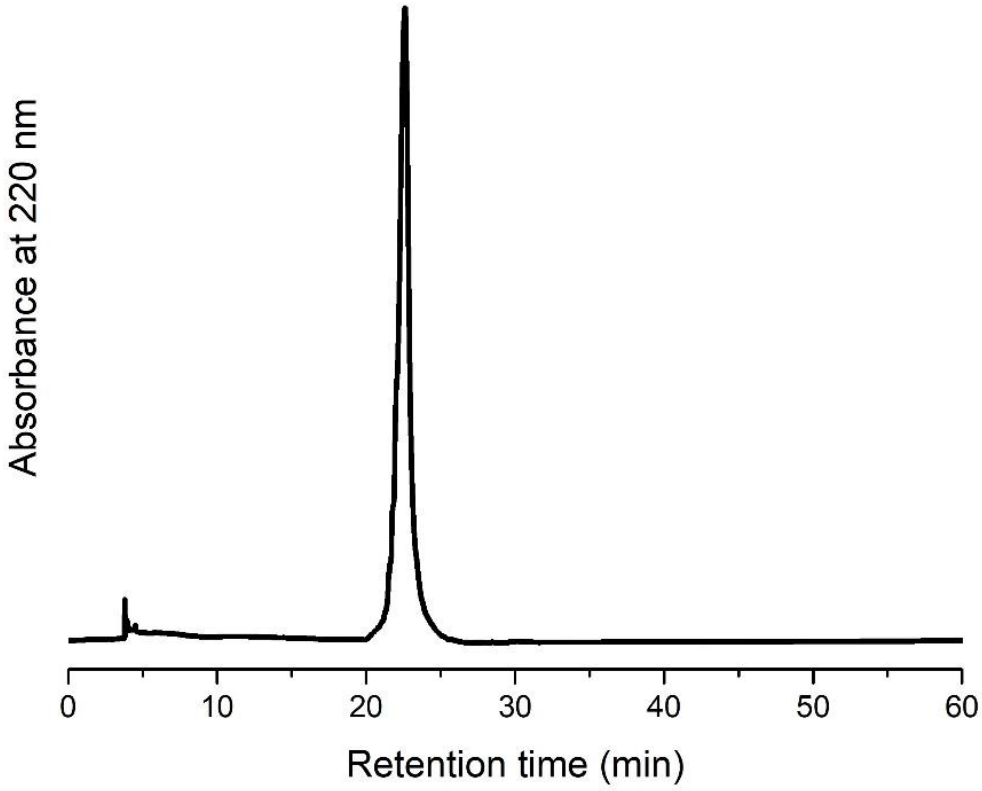

(b)

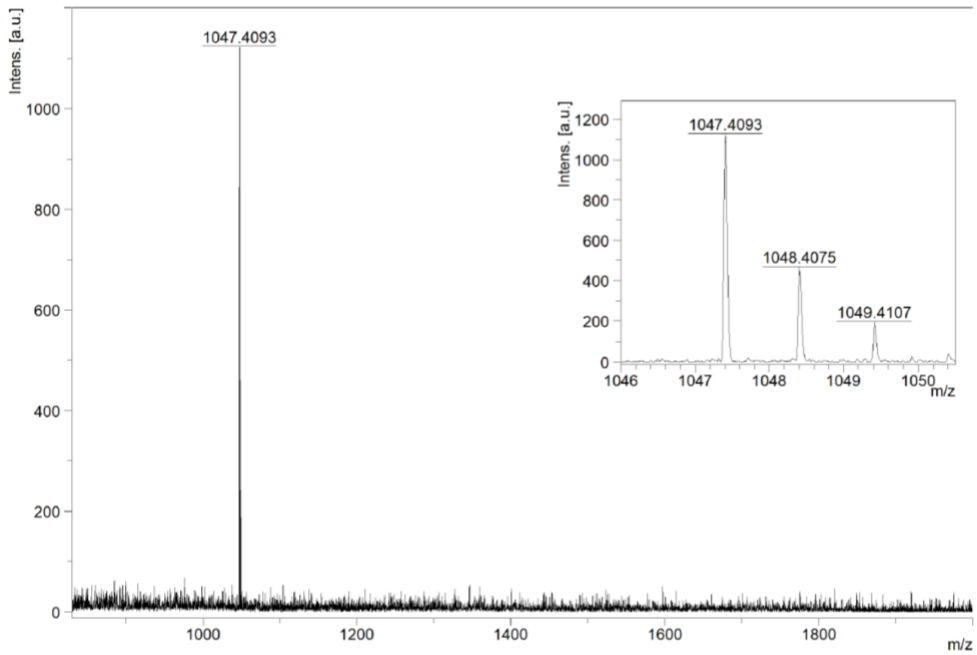

Figure S3. (a) HPLC chromatogram and (b) MALDI-TOF mass spectrum of **cRGD-OPA**.

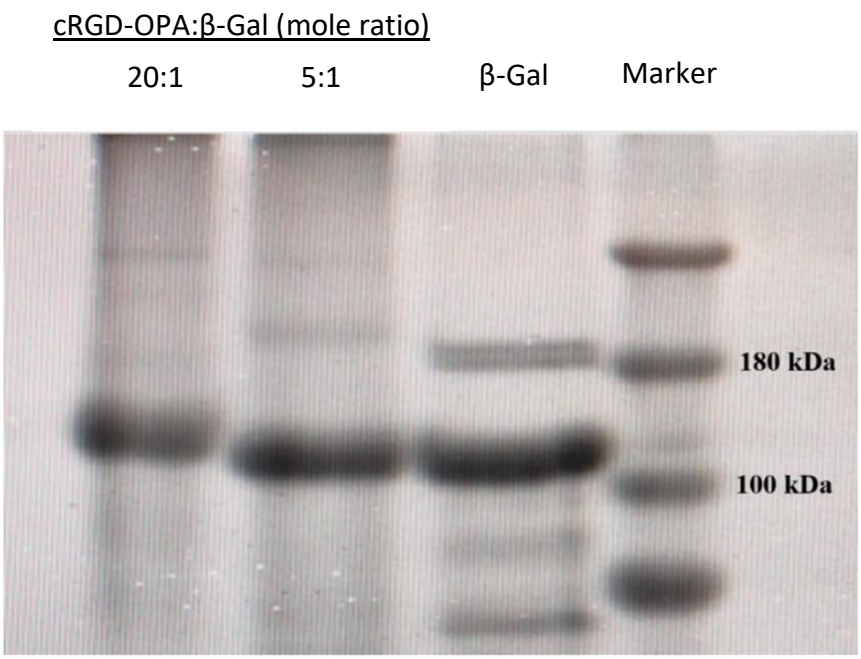

Figure S4. SDS-PAGE analysis of the native β-Gal and β-Gal conjugated with different mole ratios of **cRGD-OPA**.

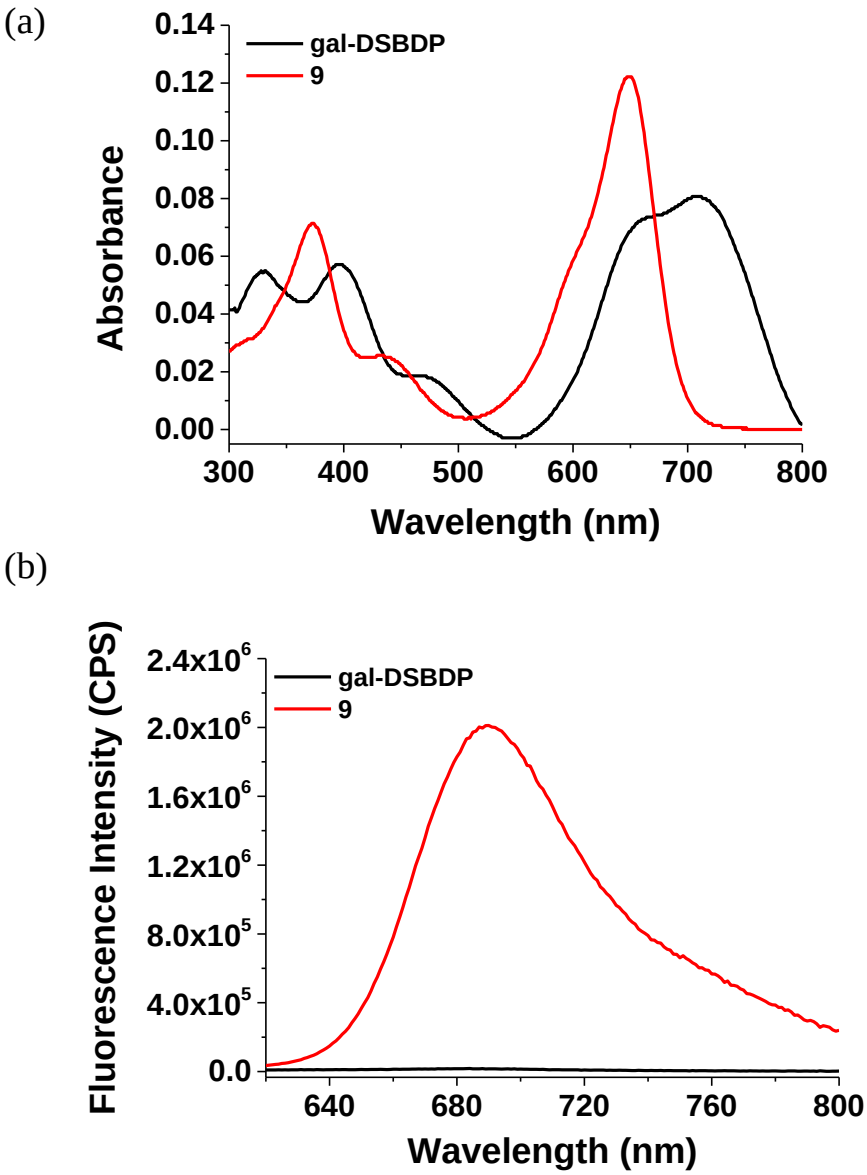

Figure S5. (a) Electronic absorption and (b) fluorescence (λ_{ex} = 610 nm) spectra of **gal-DSBDP** and **9** (both at 2 μM) in PBS (pH 7.4) with 10% DMSO (v/v).

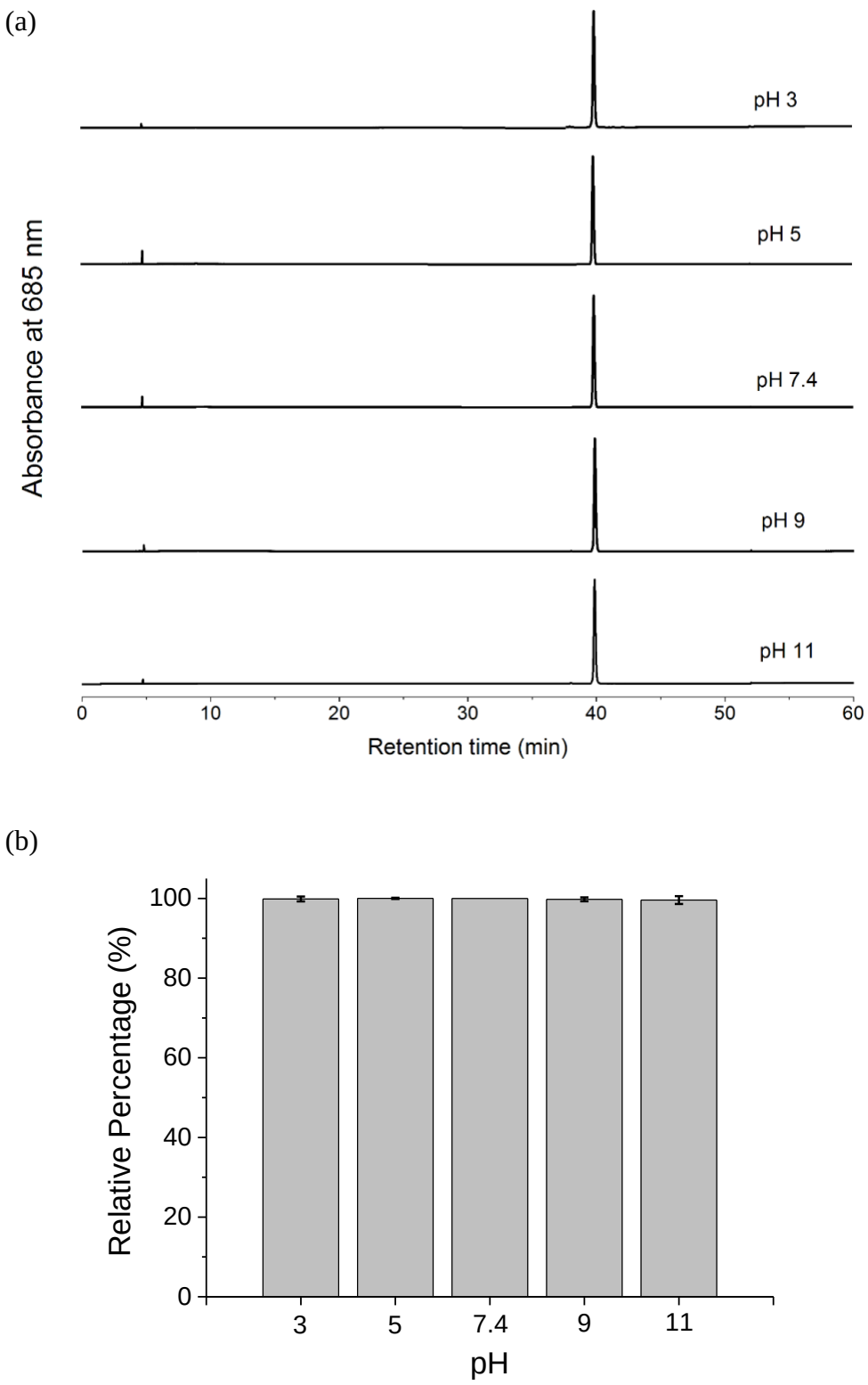

Figure S6. (a) HPLC chromatograms of **gal-DSBDP** in PBS with 10% DMSO (v/v) at different pH. (b) Relative percentages of **gal-DSBDP** under different conditions as determined by integrating the peak areas in the HPLC chromatograms. Data are expressed as the mean ± SD of three independent experiments.

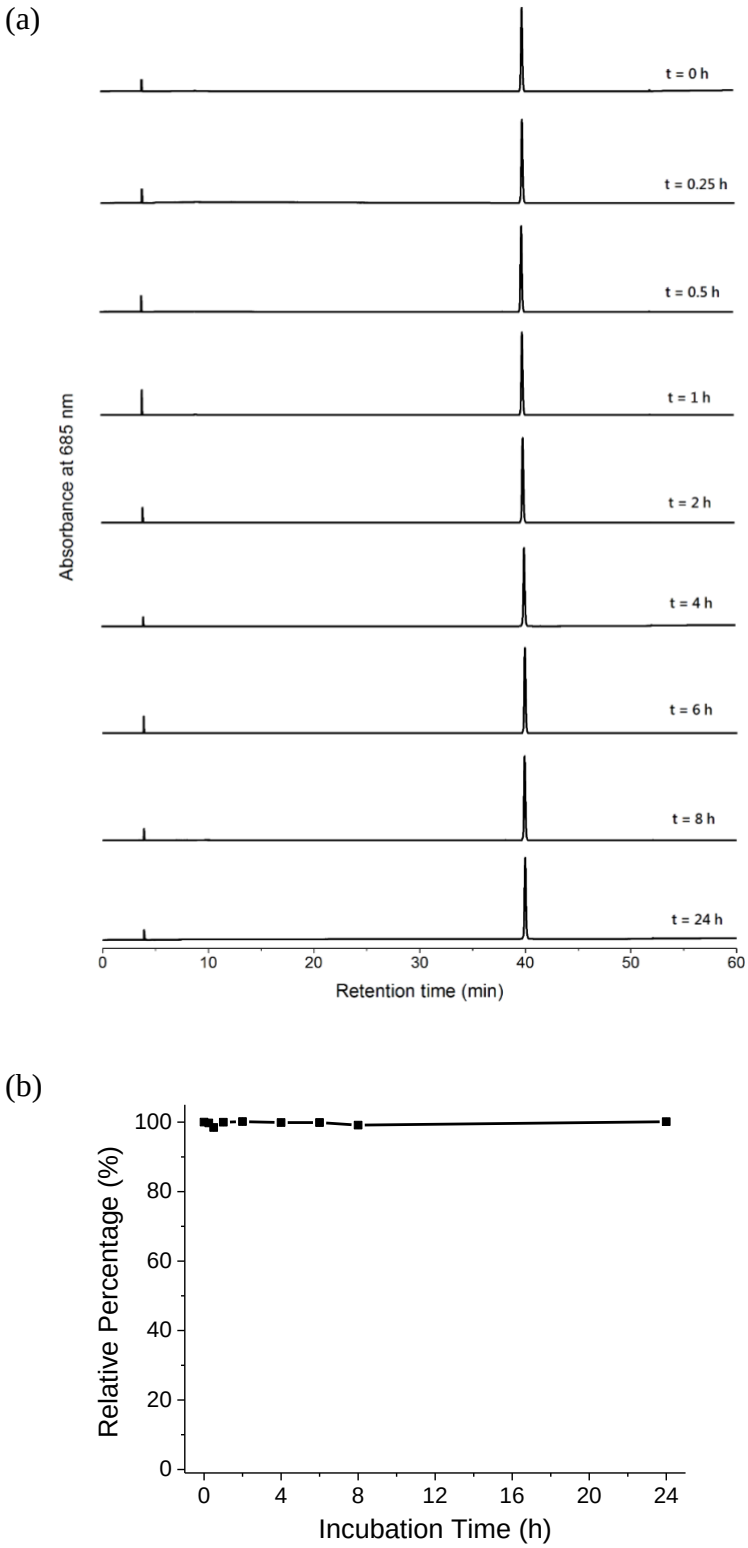

Figure S7. (a) HPLC chromatograms of **gal-DSBDP** in DMEM with 20% FBS (v/v) and 10% DMSO (v/v) at 37 °C over a period of 24 h. (b) Relative percentages of **gal-DSBDP** at different time points as determined by integrating the peak areas in the HPLC chromatograms. Data are expressed as the mean ± SD of three independent experiments.

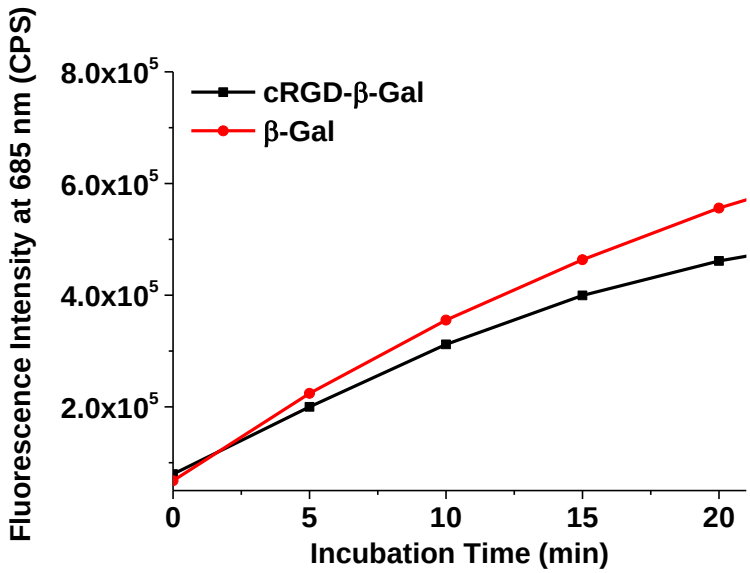

Figure S8. Change in fluorescence intensity at 685 nm for **gal-DSBDP** (2 μM) upon treatment with the native β-Gal or **cRGD-β-Gal** (6 unit mL^{-1}) in PBS (pH 7.4) with 10% DMSO (v/v) at 37 ^{o}C with the incubation time.

(a)

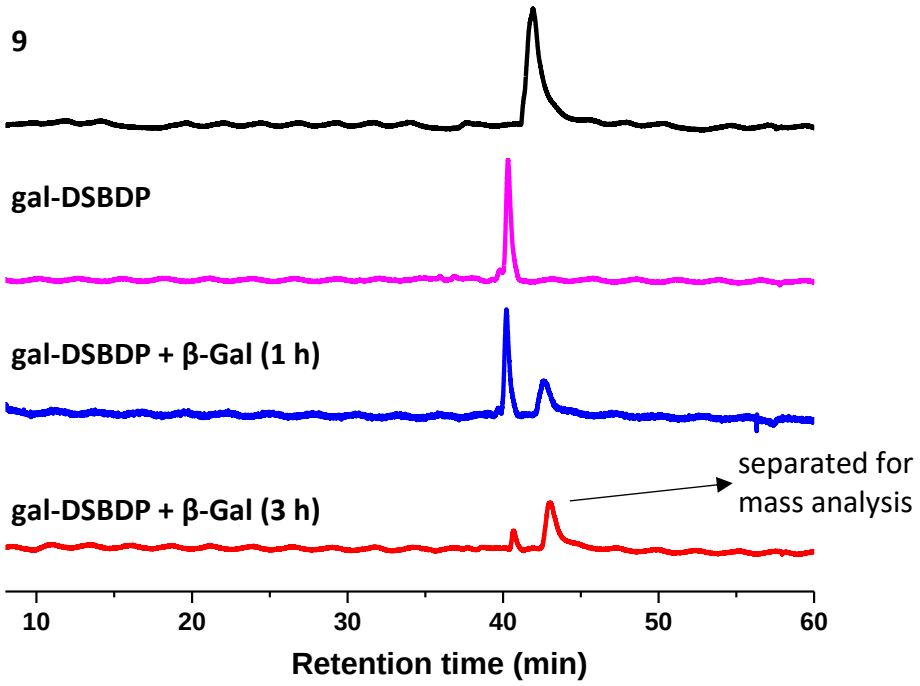

(b)

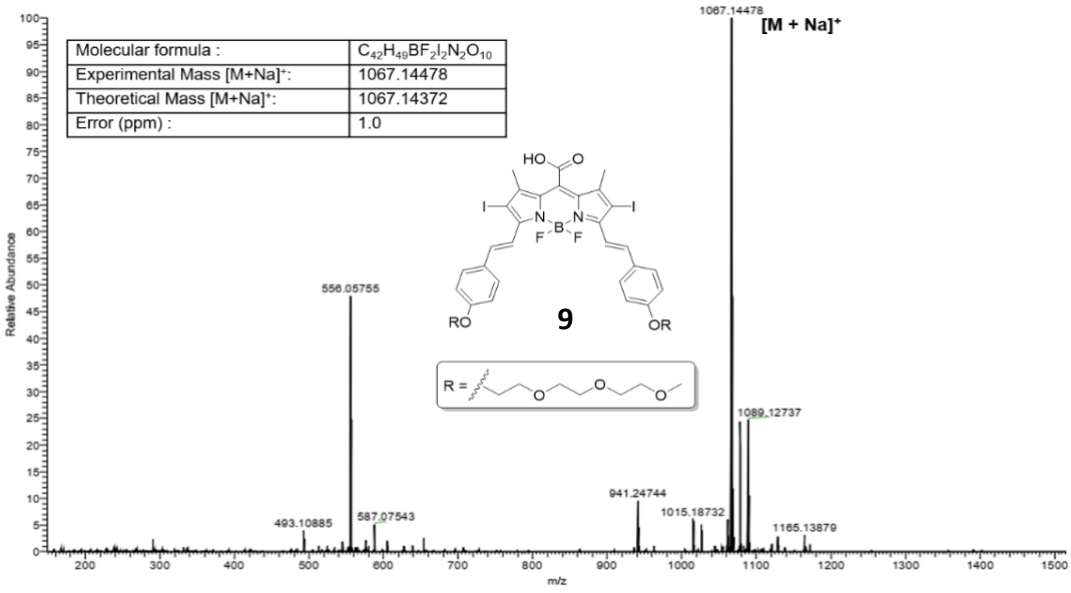

Figure S9. (a) HPLC chromatograms of **9**, **gal-DSBDP**, and their mixture in PBS (pH 7.4) with 10% DMSO (v/v) at 37 °C after 1 h and 3 h. (b) ESI mass spectrum of the isolated fraction with a retention time of ca. 44 min.

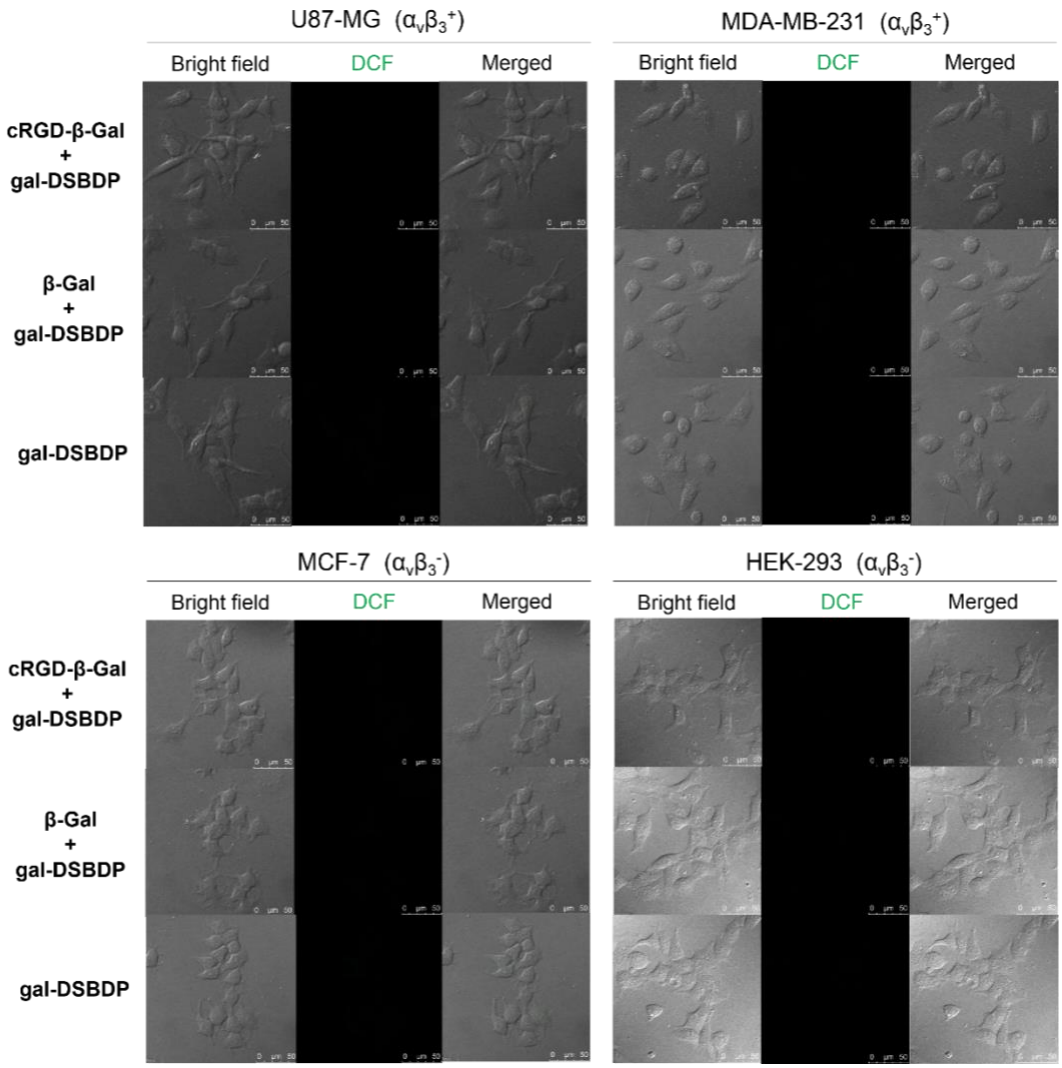

Figure S10. Intracellular ROS production as reflected by the intracellular fluorescence intensity of DCF in U87-MG, MDA-MB-231, MCF-7, and HEK-293 cells after incubation with **gal-DSBDP** (4 μM) for 30 min with or without preincubation with **cRGD-β-Gal** or β-Gal (10 unit mL^{-1}) for 1 h, followed by post-incubation in a drug-free medium for further 3 h and then with H_2DCFDA (10 μM) for 30 min under a dark condition.

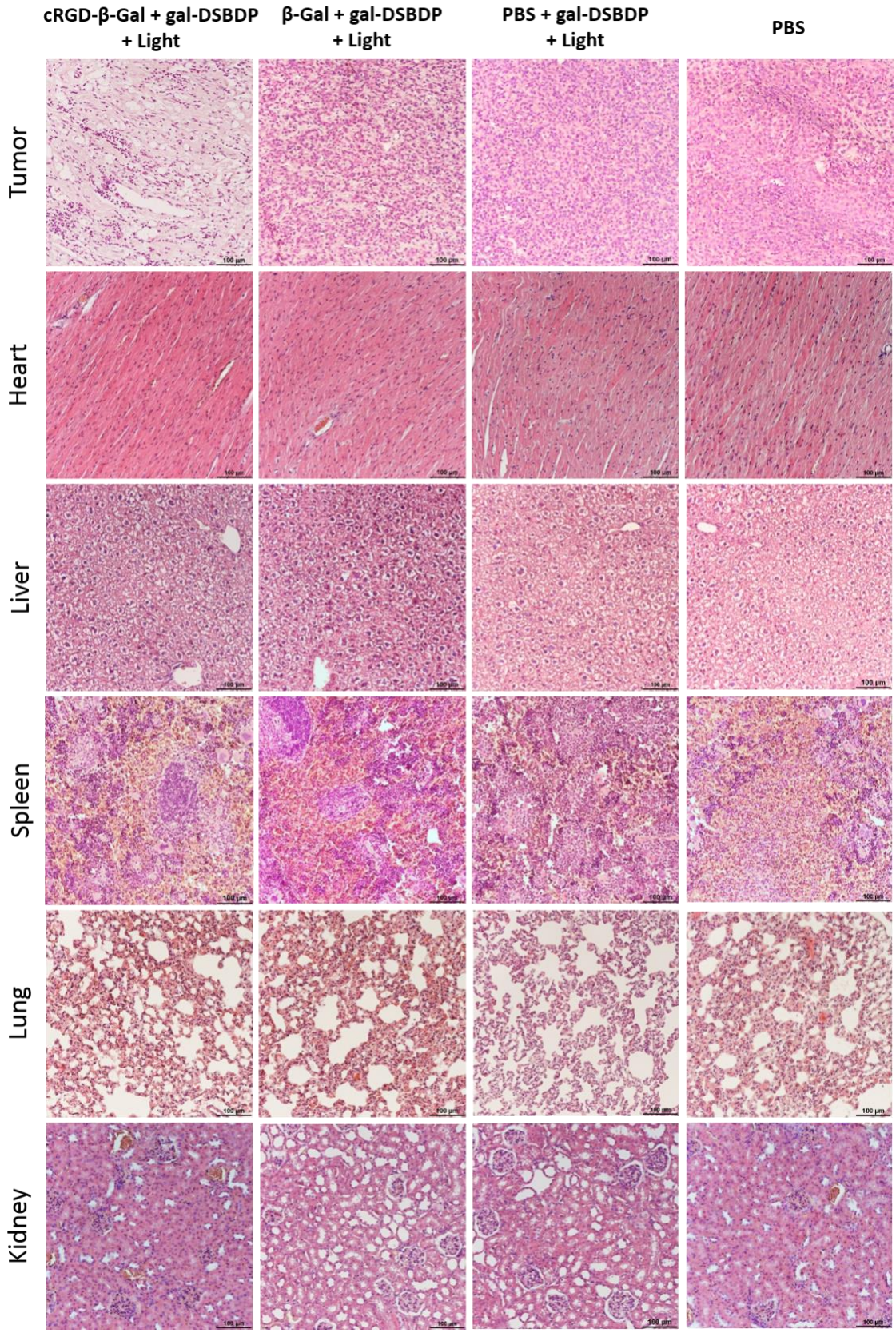

Figure S11. H&E-stained slices of the tumor and major organs of the mice at Day 14 after the different treatments.

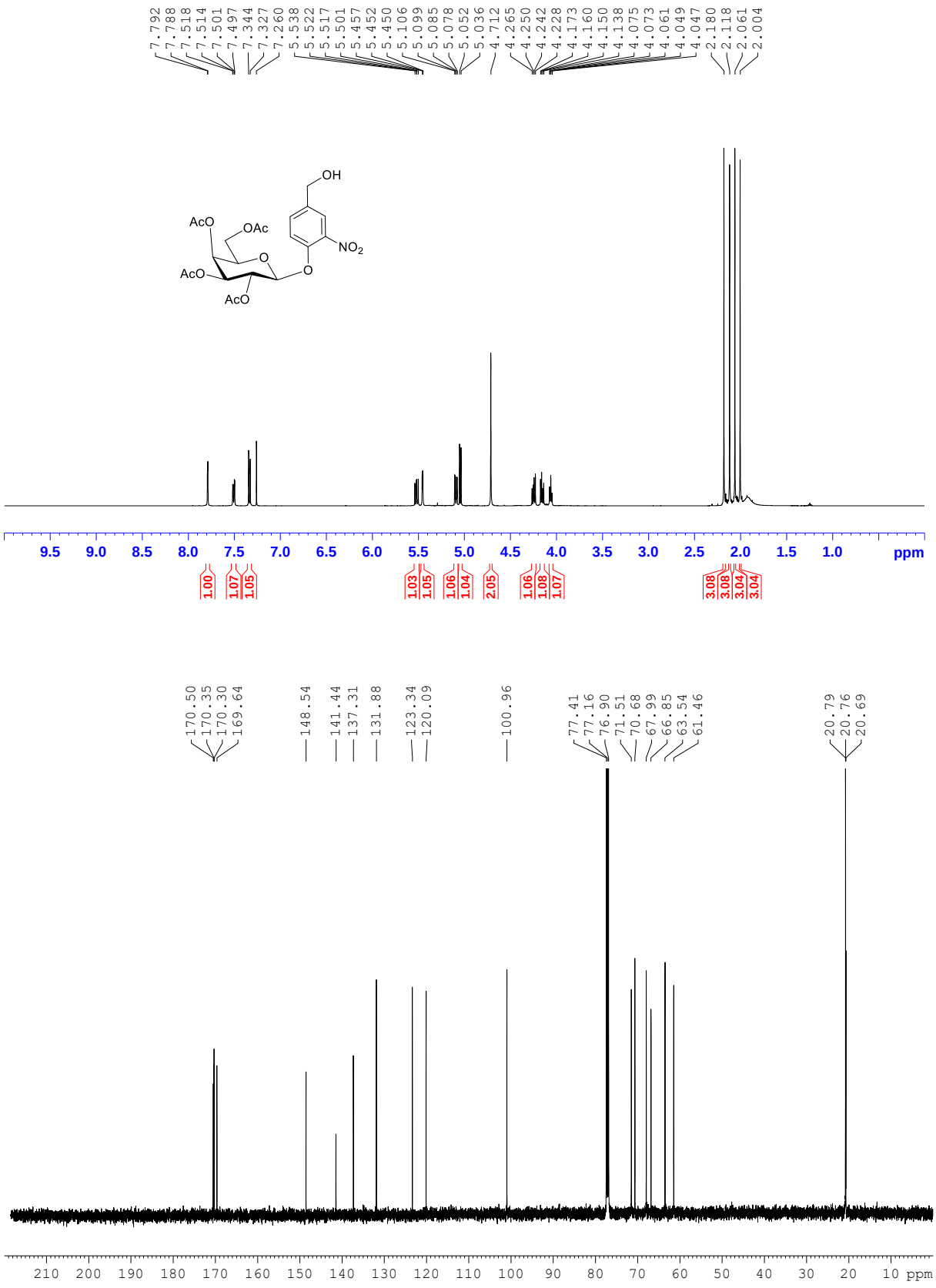

Figure S12. ^{1}H (top) and $^{13}C\{^{1}H\}$ (bottom) NMR spectra of **3** in $CDCl_3$.

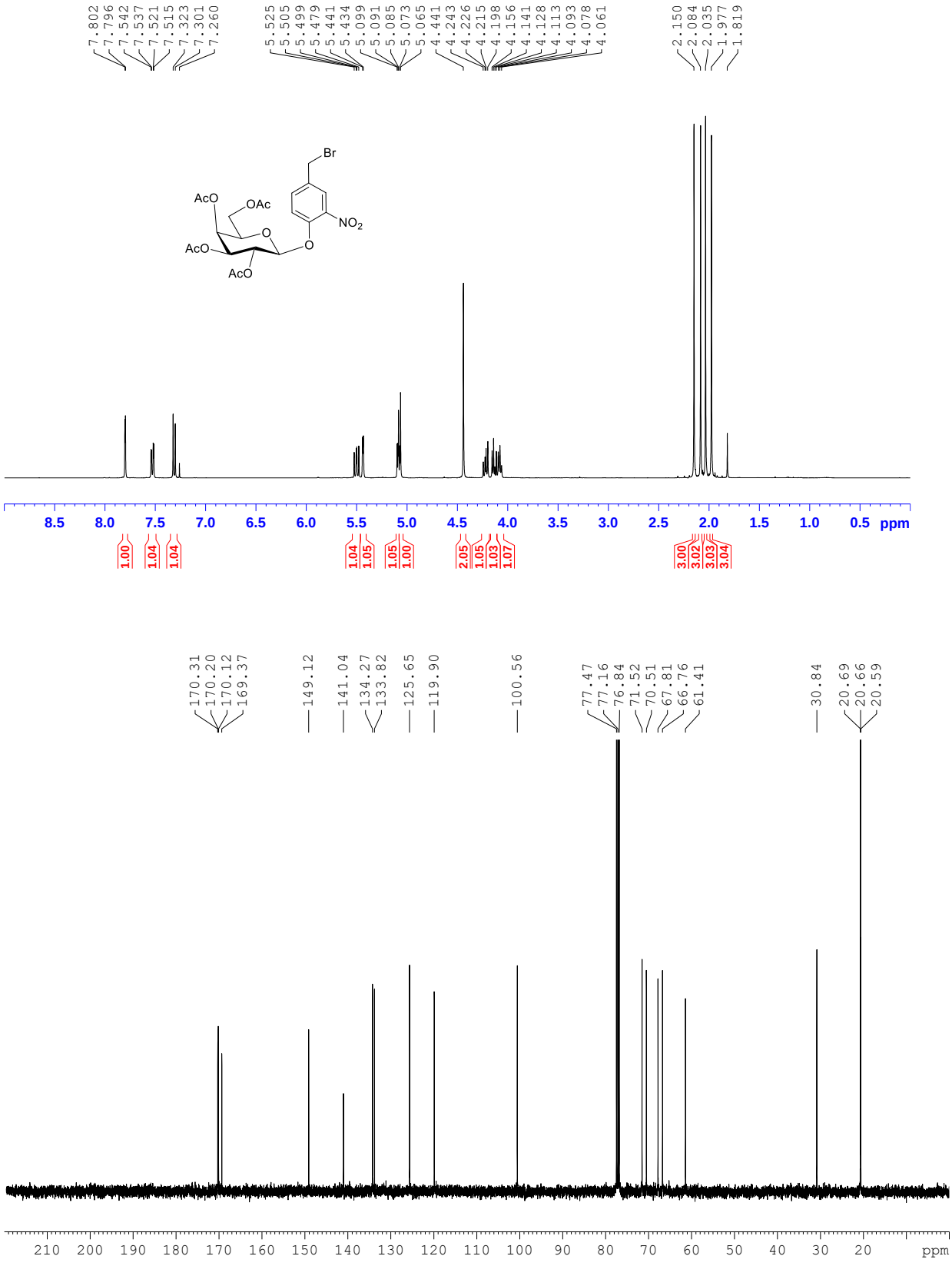

Figure S13. ^{1}H (top) and $^{13}C\{^{1}H\}$ (bottom) NMR spectra of **4** in $CDCl_3$.

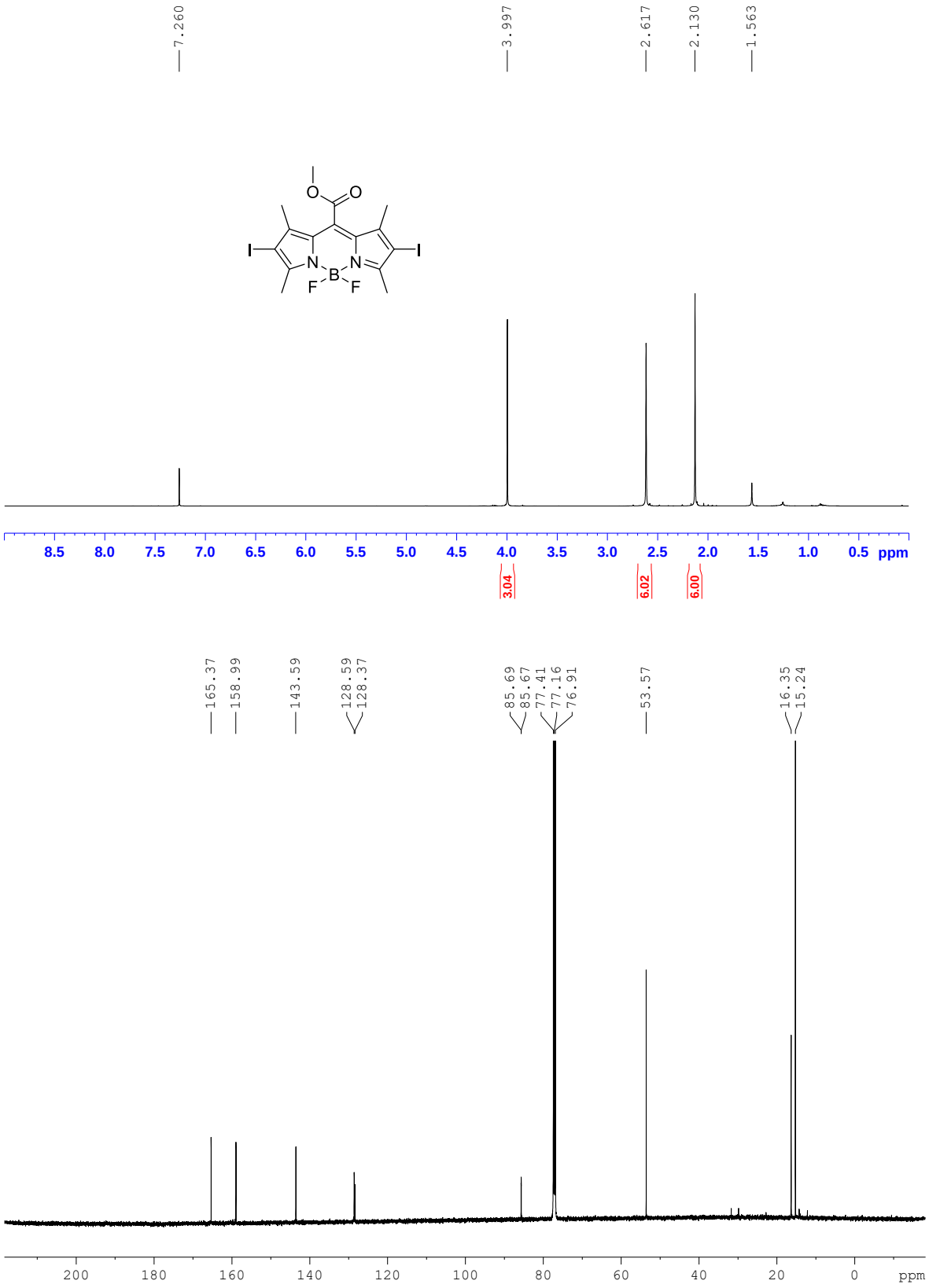

Figure S14. ^{1}H (top) and $^{13}C\{^{1}H\}$ (bottom) NMR spectra of **6** in $CDCl_3$.

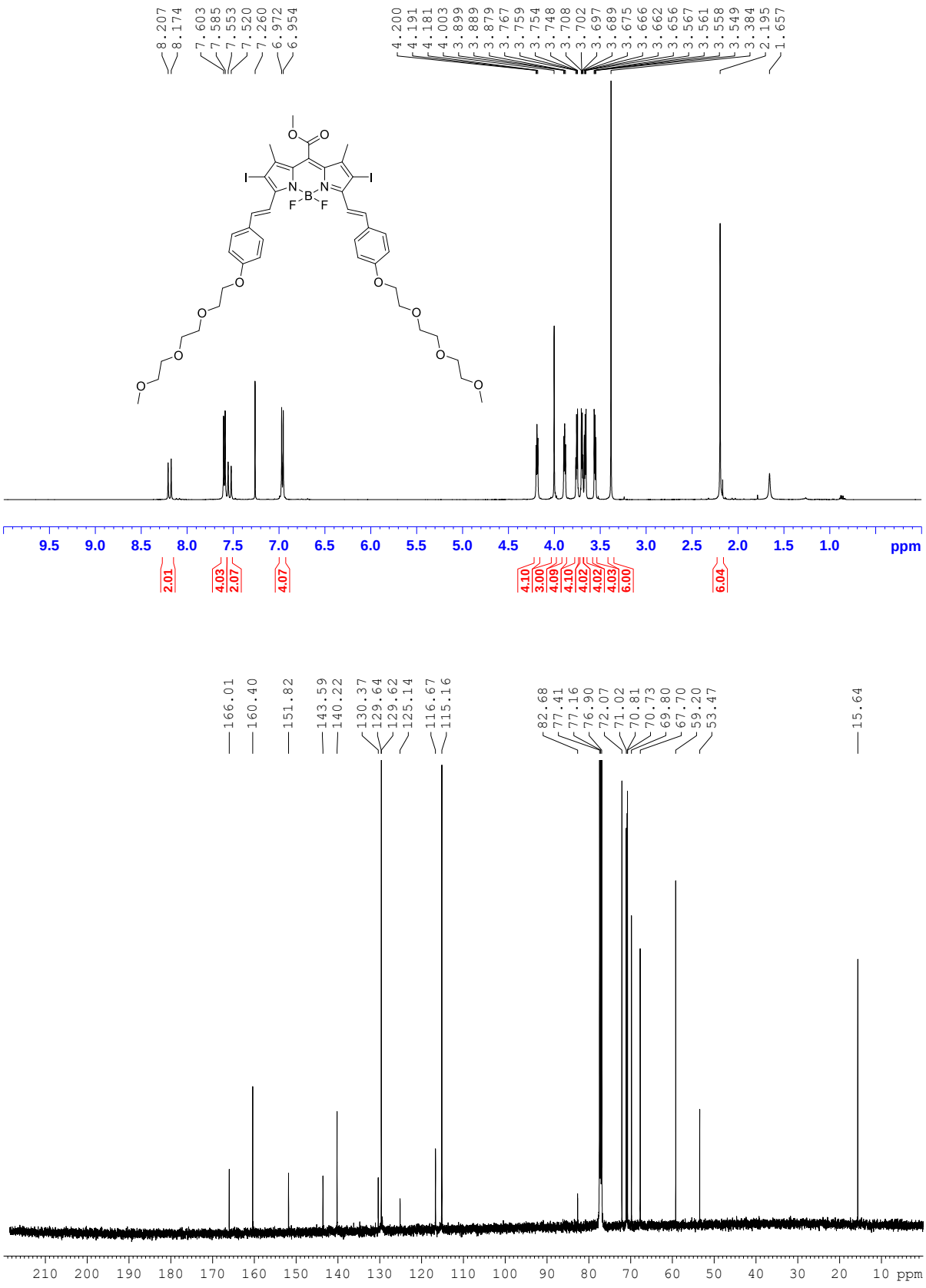

Figure S15. ^{1}H (top) and $^{13}C\{^{1}H\}$ (bottom) NMR spectra of **8** in $CDCl_3$.

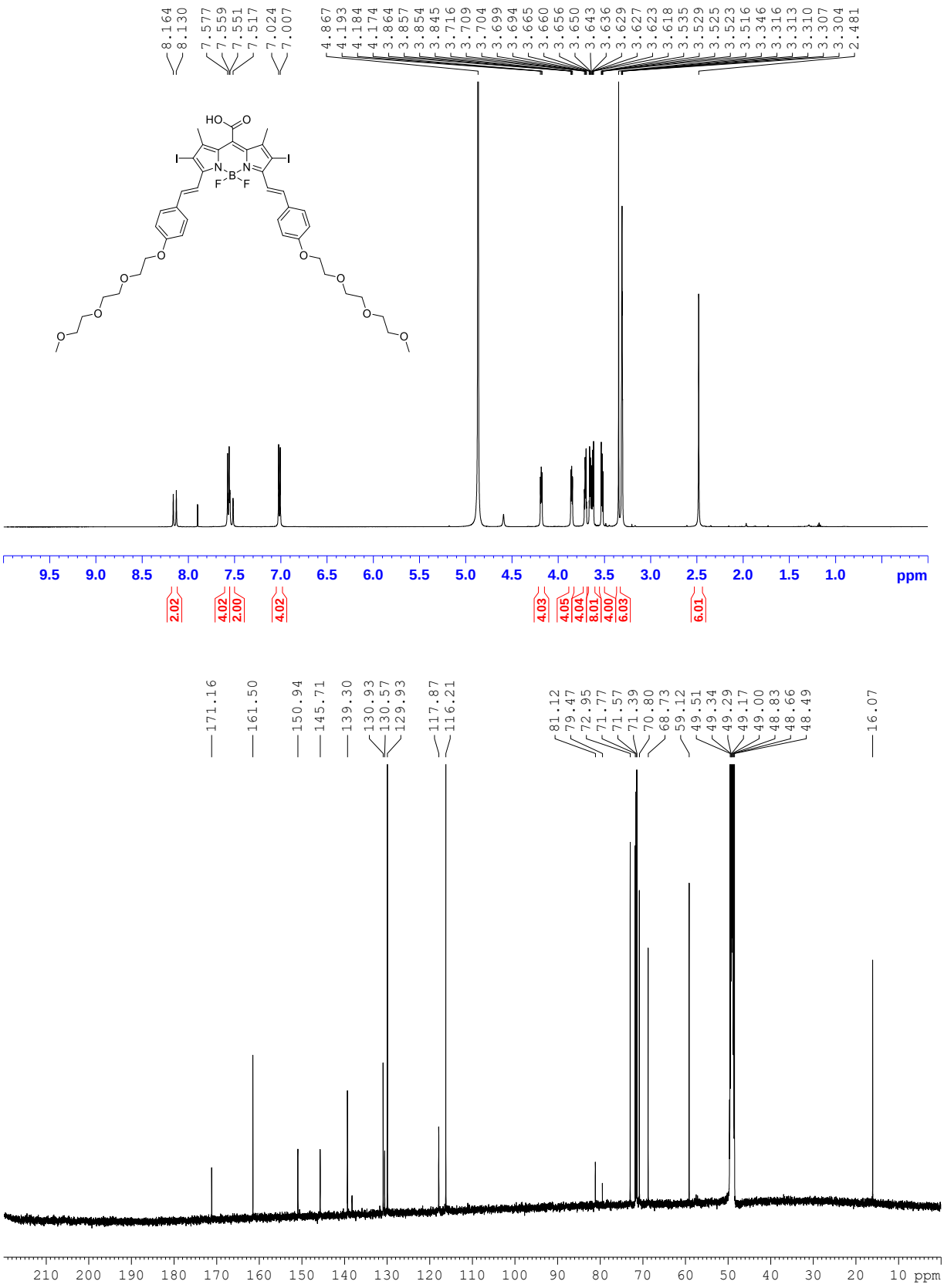

Figure S16. ^{1}H (top) and $^{13}C\{^{1}H\}$ (bottom) NMR spectra of **9** in CD_3OD.

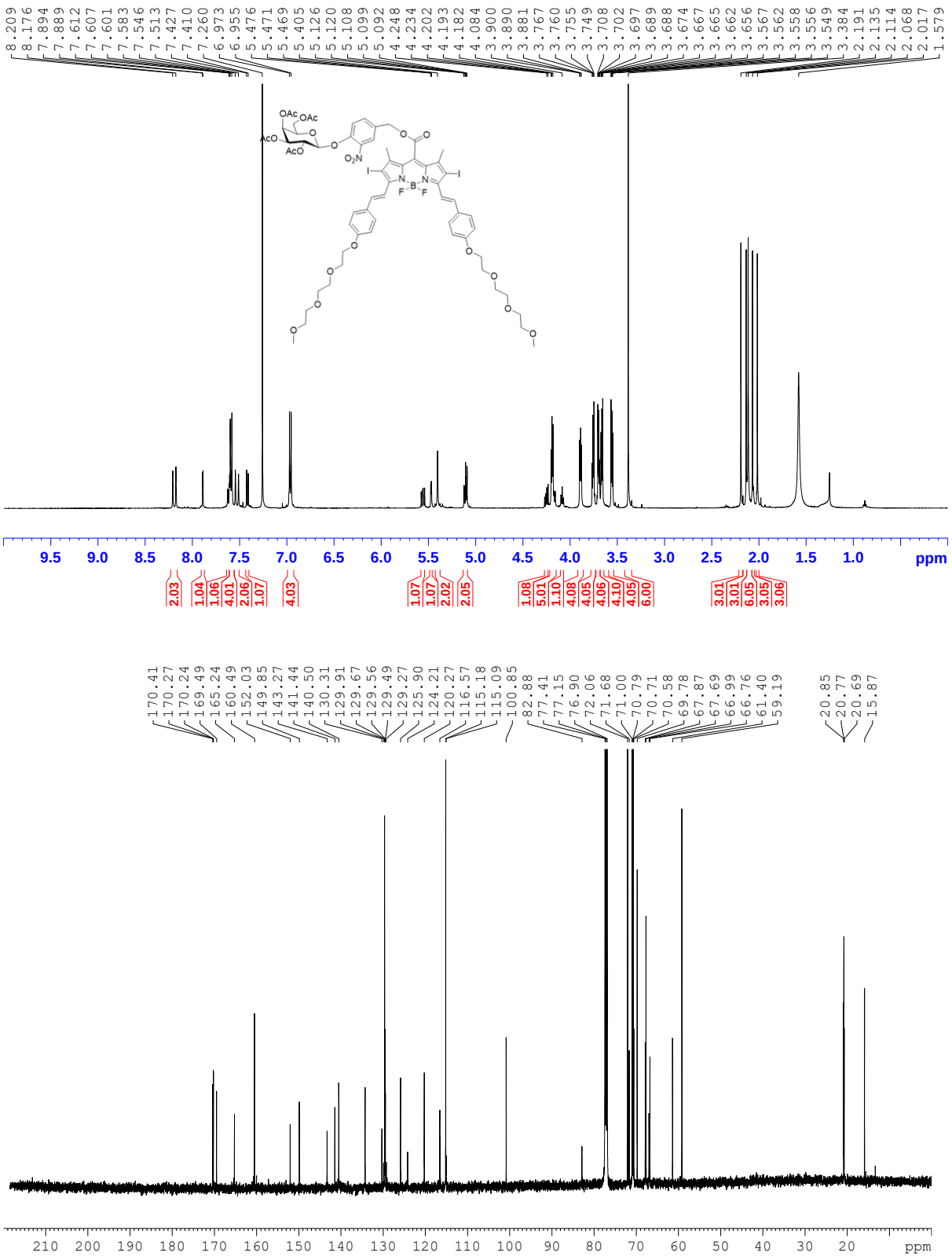

Figure S17. ^{1}H (top) and $^{13}C\{^{1}H\}$ (bottom) NMR spectra of **10** in $CDCl_3$.

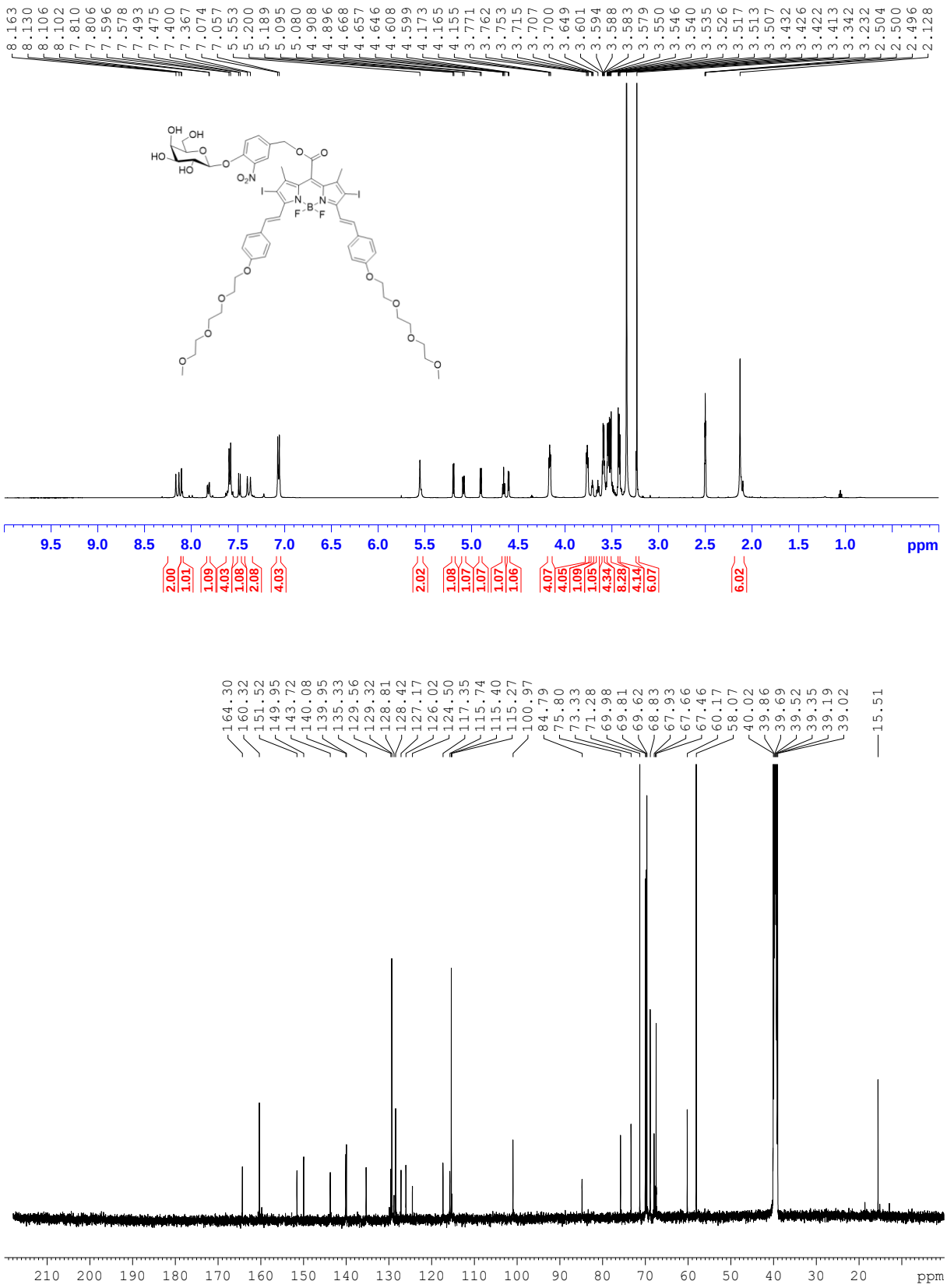

Figure S18. ^{1}H (top) and $^{13}C\{^{1}H\}$ (bottom) NMR spectra of **gal-DSBDP** in DMSO-d_6.

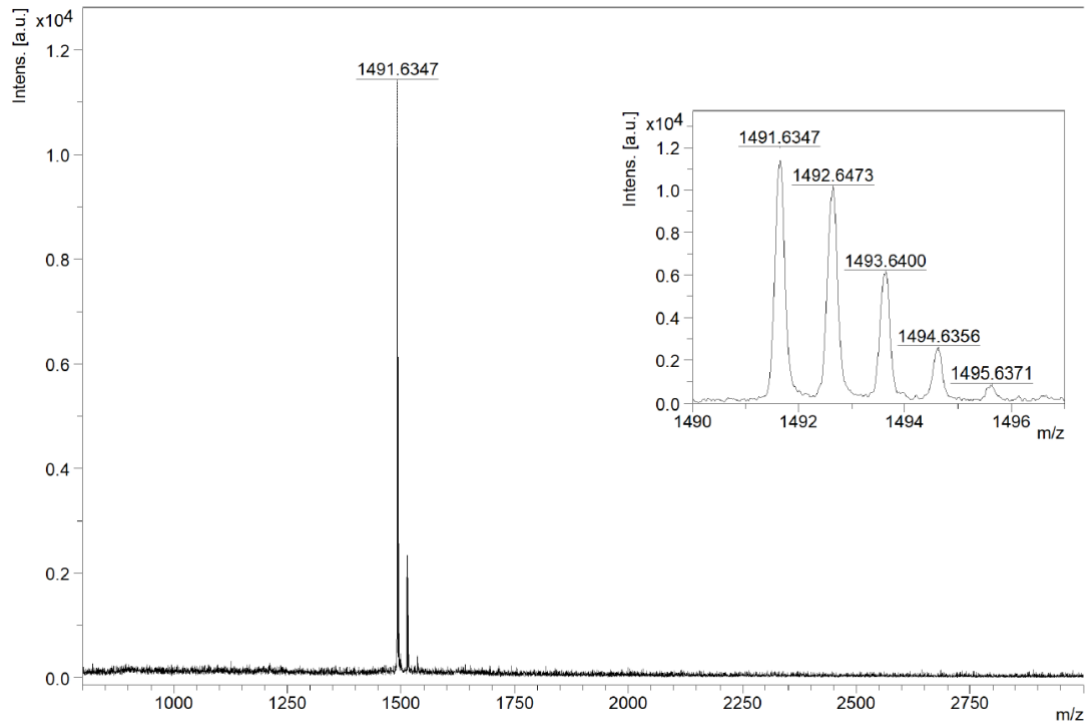

Figure S19. MALDI-TOF mass spectrum of **EBP**.

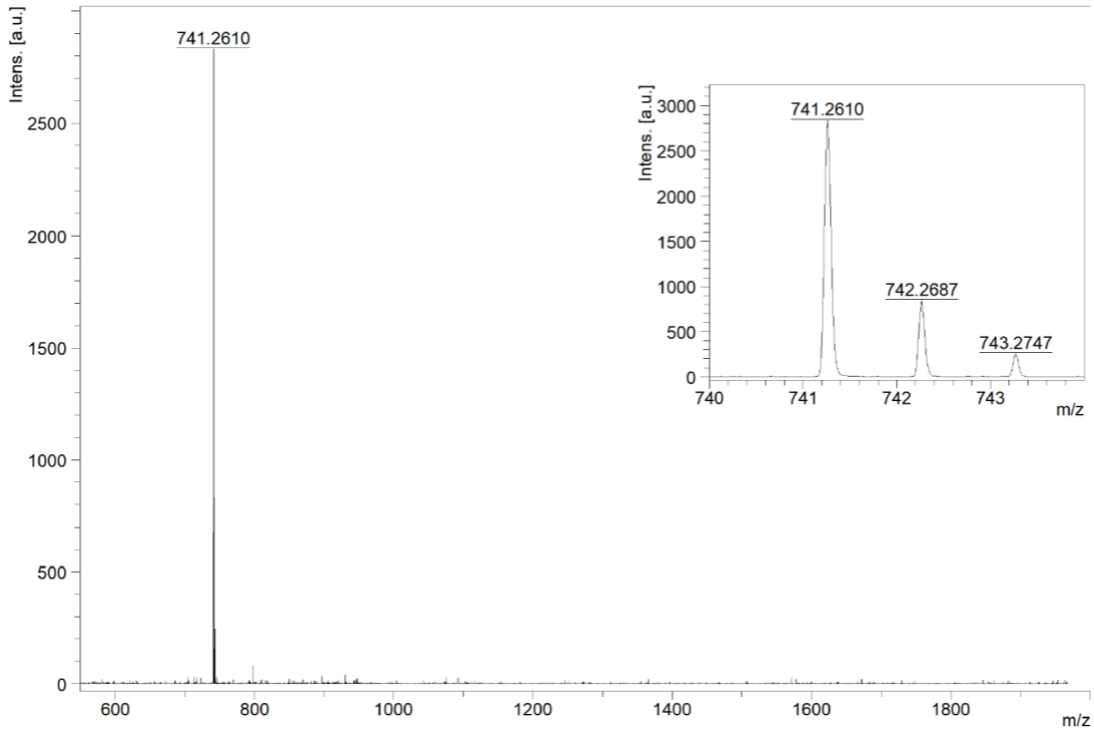

Figure S20. MALDI-TOF mass spectrum of **RGD**.

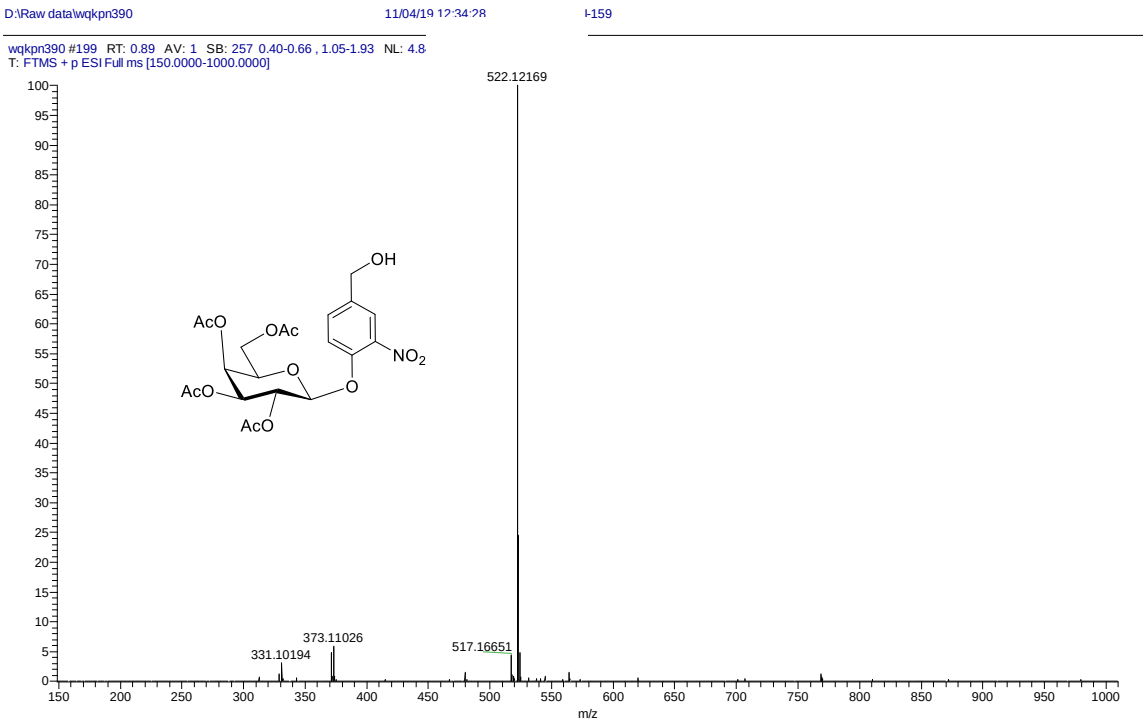

Figure S21. ESI mass spectrum of **3**.

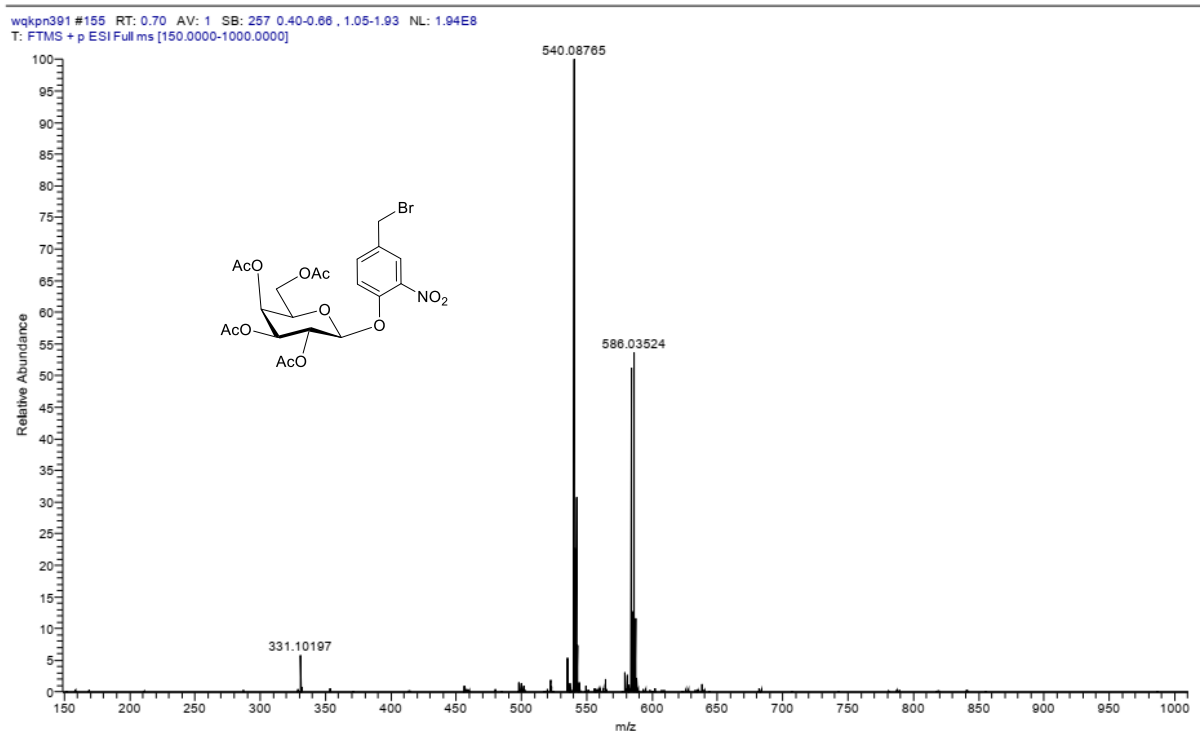

Figure S22. ESI mass spectrum of **4**.

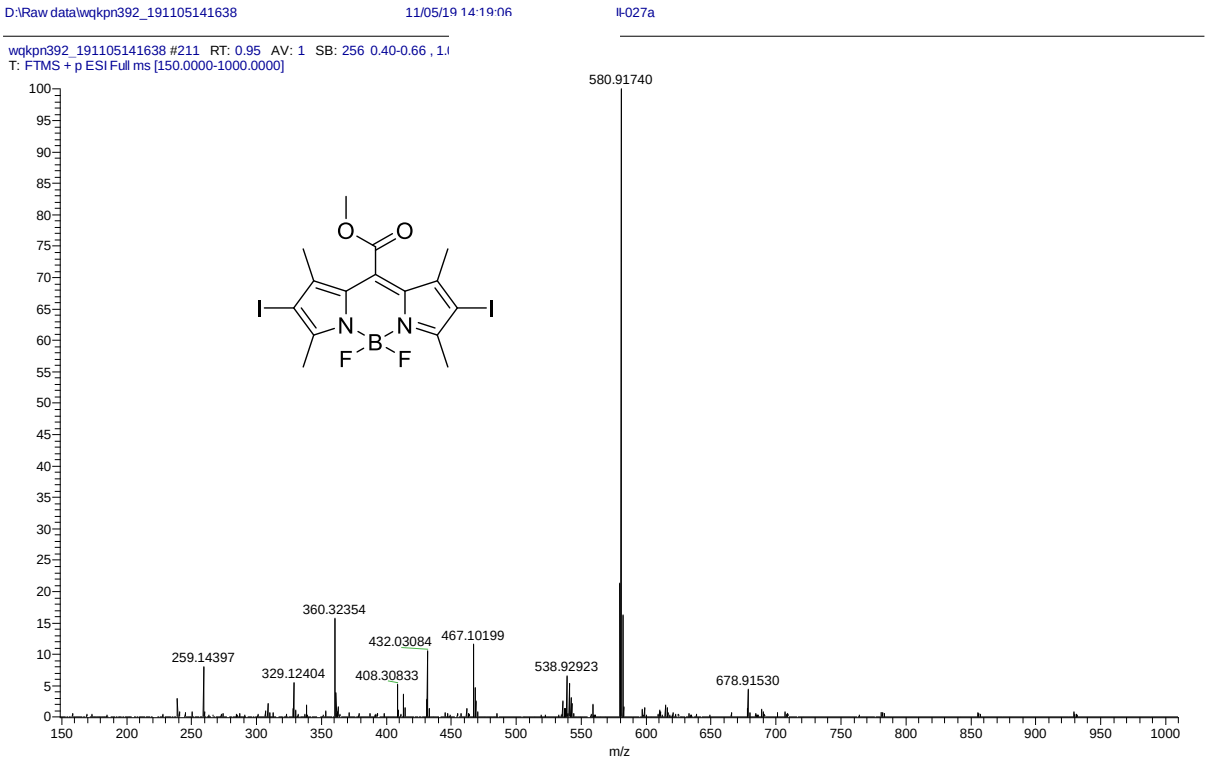

Figure S23. ESI mass spectrum of **6**.

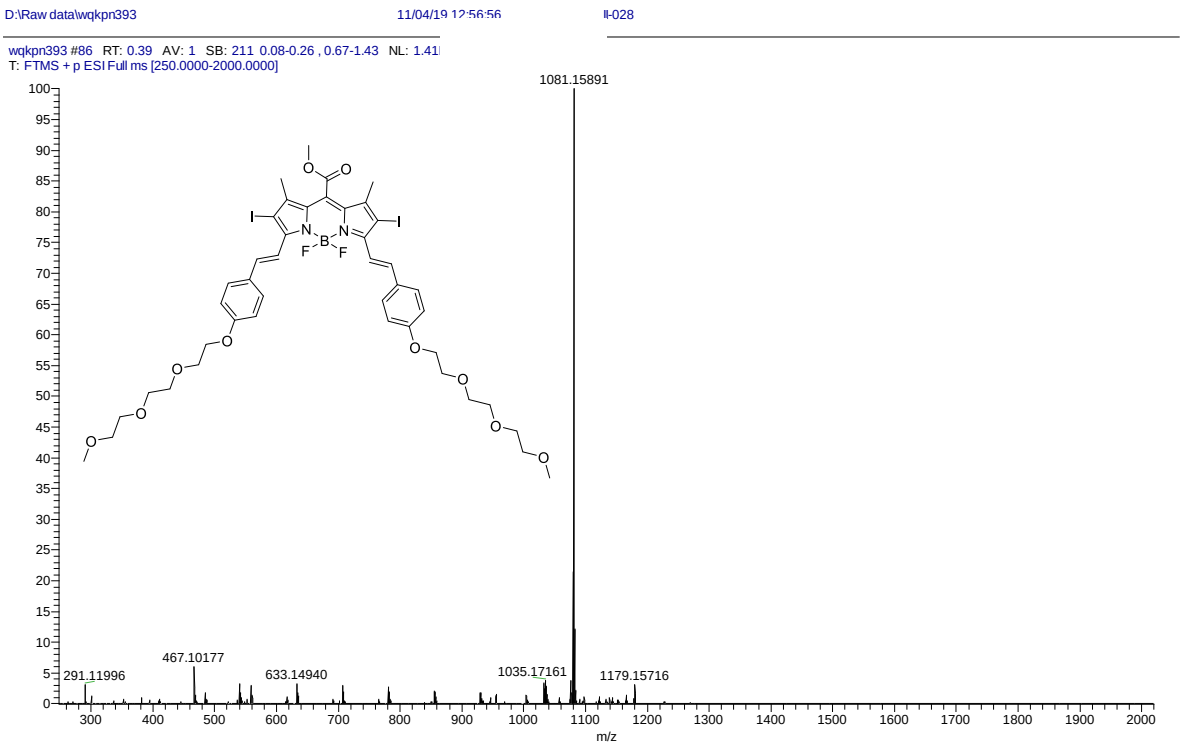

Figure S24. ESI mass spectrum of **8**.

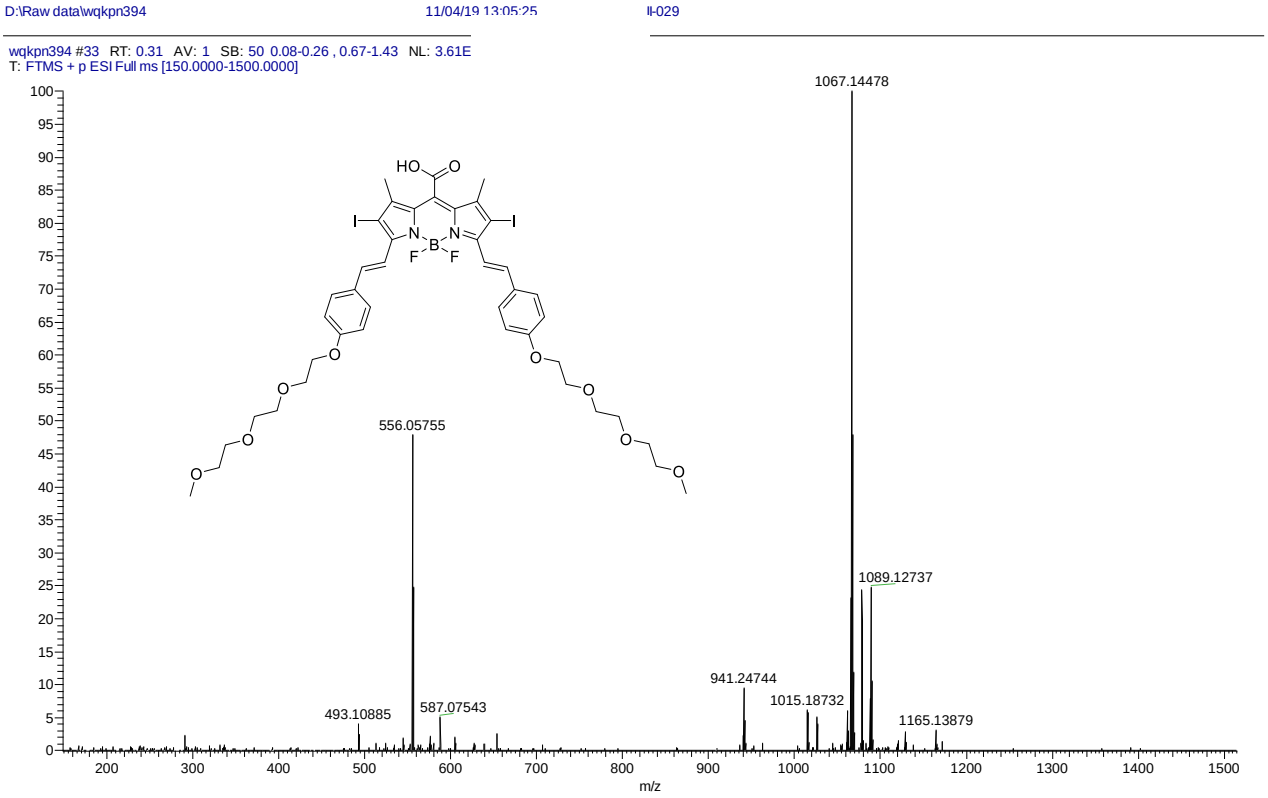

Figure S25. ESI mass spectrum of **9**.

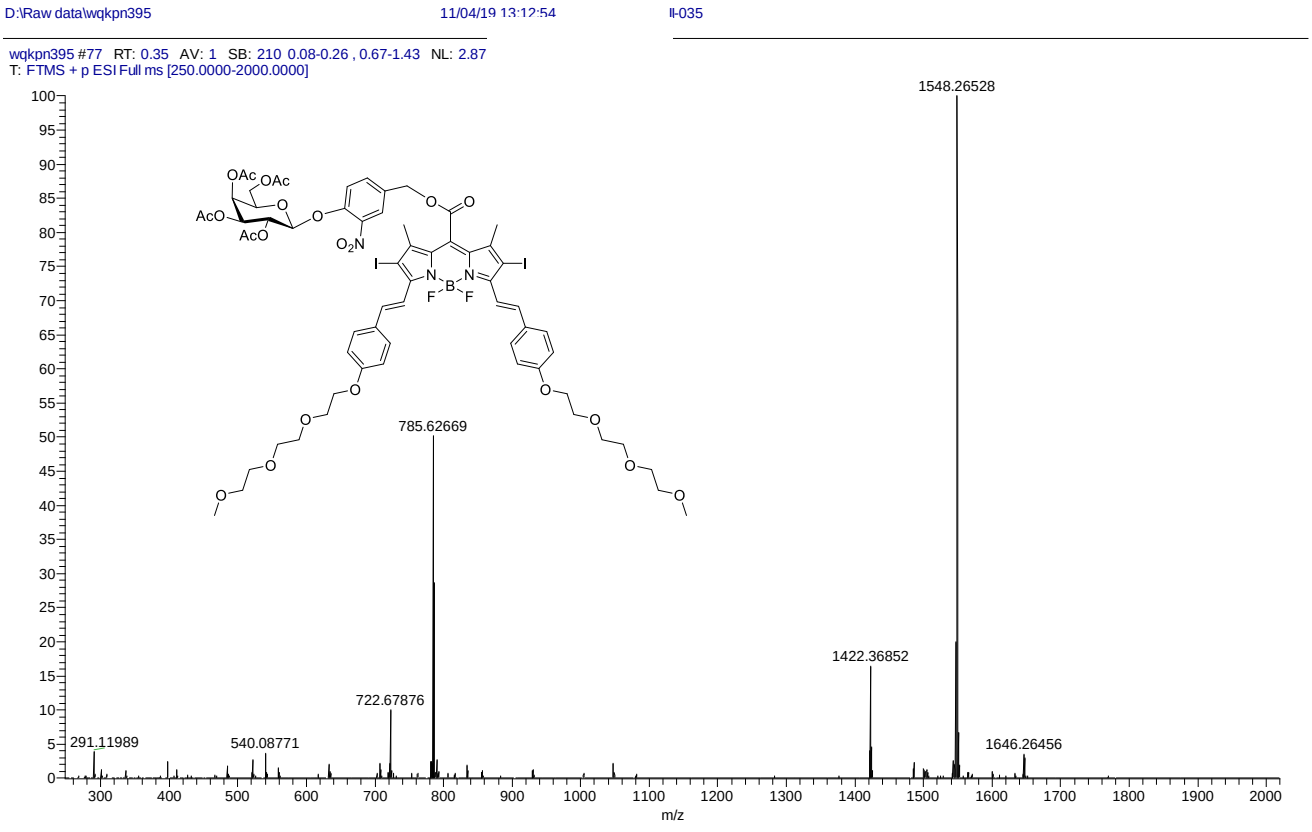

Figure S26. ESI mass spectrum of **10**.

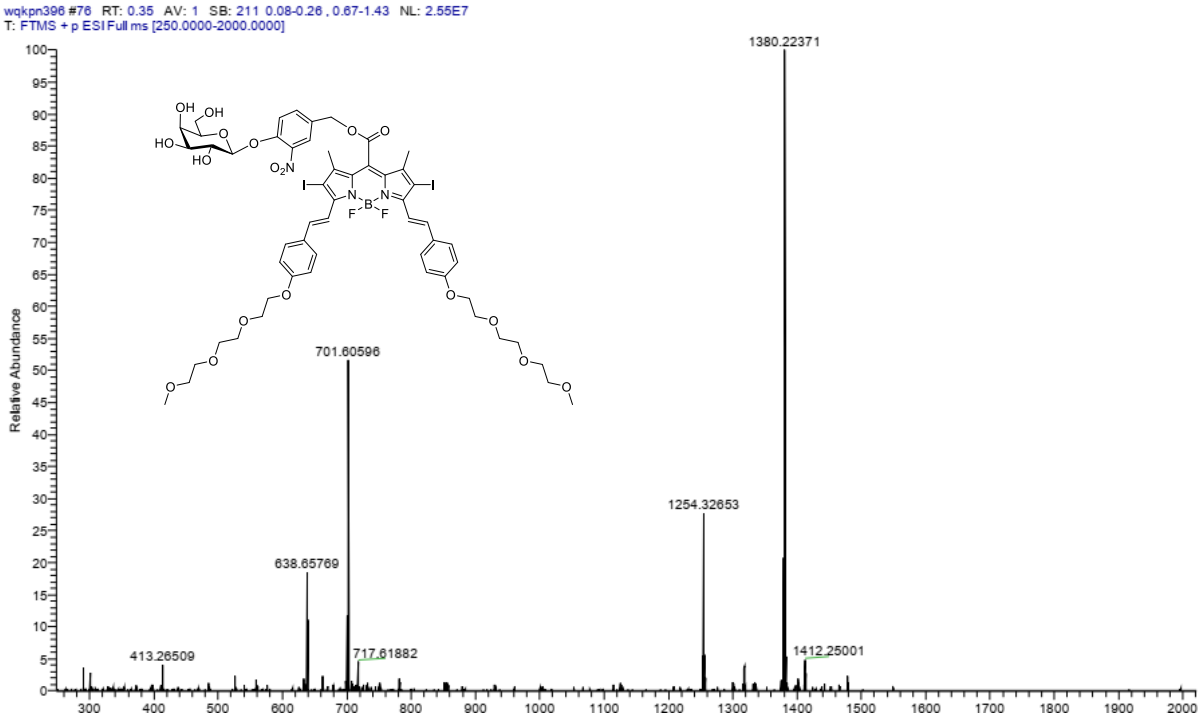

Figure S27. ESI mass spectrum of **gal-DSBDP**.